DEGREE PROJECT IN MECHANICAL ENGINEERING,
SECOND CYCLE, 30 CREDITS
STOCKHOLM, SWEDEN 2018

Application of the open source code Nemoh for modelling of added mass and damping in ship motion simulations

EMIL ANDERSSON

KTH ROYAL INSTITUTE OF TECHNOLOGY
SCHOOL OF ENGINEERING SCIENCES

Abstract

Two different numerical tools were considered, the first one is a seakeeping method developed by KTH Ship Dynamics Research Program. It utilizes strip theory and Lewis forms and is further addressed as *SMS*. The second one, *Nemoh* is an open source code utilizing three-dimensional panel method for calculating first order hydrodynamic coefficients in the frequency domain.

A comprehensive revision of *Nemoh* and *SMS* has been performed on behalf of the KTH Ship Dynamics Research Program. The background to the revision was the high interest in accurately capturing a ships dynamic response. The aim was to explore the prospect of making use of the open source code *Nemoh* for modelling of added mass and damping in terms of modelling, computational efforts and ship motion prediction improvements. Further, the thesis includes a well-described method on how to operate and pre-process data for *Nemoh* together with a validation study including results from commercial software´s and experimental studies. An approach with the aim to capture the speed-dependency of the hydrodynamic coefficients together with further potential development of *Nemoh* is addressed.

The validation of *Nemoh* is showing diverse result. For two cases, the Response Amplitude in Heave is insufficiently modelled. In consequence it's stated that further studies are required in order to establish whether it's the case of inadequate input from the authors' side or lack of robustness in *Nemoh* that is the cause. The approach to capture speed effects in the hydrodynamic coefficients is proven to be fairly accurate and is considered to be of further use for future development of *Nemoh.*

With respect to identified computational efforts, it's concluded that *Nemoh* requires much more computational time than *SMS* while the accuracy of result is lower. No major improvements may therefore be achieved by substituting or implementing parts of *Nemoh* into *SMS*. *Nemoh* is however of use for the KTH Ship Dynamics Research Program and of other users of Lewis Method when establishing whether a hull-geometry is considered to be "too" unconventional for a two-parameter mapping technique or not. The capability to calculate the RAO in surge is also of interest for KTH Ship Dynamics Research Program since it's not a feature in *SMS*.

Preface

This paper is a Master Thesis at the Centre of Naval Architecture at the Department of Aeronautical and Vehicle Engineering at KTH, Royal Institute of Technology in Stockholm. The thesis was initiated by KTH Ship Dynamics Research Program and supervised by Dr. Anders Rosén, KTH and Erik Ovegård, StormGeo.

I would like to thank my supervisors for their excellent guidance and contribution of influential ideas. Thank you, Anders, for leading me on the right path every time I was lost within the mathematical wonders of hydrodynamic modelling. And thanks Erik for answering every question regarding the numerical problems associated with hydrodynamic modelling.

I would also like to share my gratitude to:
The colleagues at the StormGeo office in Stockholm for the interesting discussions shared regarding the EnRoute Live software.
Professor Dominic A. Hudson, for taking your time to discuss and in detail describe the methodology behind a Pulsating Source Method.

Emil Andersson
Stockholm, June 2018

Content

1. Introduction

The demand for high capacity shipping with low delivery times can be of cost for safety. Slender hull forms are built with the intention of having low fuel consumption while the capacity of cargo is maximized, which in turn may have significant impact on the vessels' stability in seas. Further, it's known that large amplitude roll motions in heavy weather is problematic. The capability to predict a ships behaviour in seas and further support operational guidance may prevent damages on cargo and structure. It is therefore of crucial importance for ship designers and operators in an early design phase and ongoing lifespan to mathematically simulate ship dynamics in order to establish a good balance between safety and efficiency.

A ship's motion is a complex coupled dynamic system in 6 degrees of freedom, i.e. forces can arise in one direction due to a motion in another. In order to determine a ships dynamic response in waves, it's necessary to estimate these forces together with other hydrodynamic quantities. Forces that are acting on the ship from the surrounding environment may be divided into a hydrostatic and a hydrodynamic contribution. Linear modelling of these forces and motions is generally based on the combination of two simplified models, one when the ship is restrained from motion and subjected to waves and the second implies forced oscillations to the ship.

The excitation forces in the restrained model is in turn divided in two parts: excitation forces occurring from the undisturbed pressure acting on the hull and the pressures due to the disturbance of flow. In the case of forced oscillation, the resulting hydrostatic force may be referred to as a restoring force for which tend to bring a ship back toward a position of equilibrium. Waves will be radiating from the oscillating ship, resulting in an added-water mass and energy dispersion. The dispersed energy from the ships motion to the waves is also known as the damping of a ship and the amount fluid accelerated with the ship is referred to as the added-water mass. There exist a wide variety of software's and tools to compute a ships dynamic response in waves. The main difference between them is the mathematical method used to estimate introduced excitation forces and hydrodynamic quantities.

The first potential theory for determining hydrodynamic coefficients, such as added-mass and damping, was introduced by Ursell (1949). The published study is oriented around a so-called Strip Theory for semi-circular cross sections and has since then been further developed and implemented for ship structures. The fundamental idea behind a seakeeping method utilizing Strip Theory is to divide a ship into two-dimensional strips, assuming that there is no flow between strips. Conformal mapping techniques such as Lewis form are used to map two-dimensional strips to circular sections in order to simplify calculations. The three-dimensional quantities are obtained by integrating the two-dimensional hydrodynamic coefficients over the ship length. A further approach for determining hydrodynamic coefficients, referred to as Panel Methods was pioneered by Hess and Smith (1964). The method involves distributing sources of known frequency over panels, representing the mean wetted surface of the body and choosing a strength for the sources for which satisfies the body boundary conditions. Some of the computational methods are using linear solvers in the frequency domain, others may utilize non-linear theory in the time domain. Hybrid methods are however commonly used where non-linear effects may be implemented as a supplement to a linear analysis. Two tools of particular interest to the thesis are *SMS* and *Nemoh*, for which are shortly introduced below.

A five degree of freedom seakeeping method utilizing strip theory, referred to as *SMS*, was developed at KTH by Palmquist and Hua (1995). The hybrid method is based on linear modelling of the hydrodynamic forces using Lewis method and non-linear modelling of hydrostatic forces, Froude-Krylov forces and roll damping (de Jong 1973). The method was stripped down to a three degree of

freedom model and has since 1995 been jointly developed between KTH and StormGeo (earlier Seaware AB) where Ovegård (2009) implemented a method to capture non-linear roll phenomena in the time domain. Further, a manoeuvrability model had been implemented by Zachrisson (2011), and the work of Koskinen (2012) resulted in extension to 5 DOF simulation model. The model is very computational efficient and has proven to perform well for conventional hull-shapes. However, in the case for un-conventional hull-shapes where the midship cross-section is close to quadratic, containing sharp edges or having large beam to draught ratios, the hydrodynamic quantities of a ship might not be fully captured due to the inherent limitations of the Lewis method.

The second tool *Nemoh*, is a linear numerical solver for computation of first order hydrodynamic coefficients such as added mass, damping and excitation forces in the frequency domain (Babarit and Delhommeau 2015). The code, utilizing Panel Method, has been developed for over 30 years at École Centrale de Nantes in France and was released in open source in January 2014. It's restricted to calculations in waves for structures with zero Froude numbers i.e. zero forward speed. *Nemoh* is however poorly documented and there are no available manuals or texts of guidance, with the exception of a user's forum.

This paragraph summarizes the aim, purpose and background of the thesis. Further, a comprehensive revision of *Nemoh* and *SMS* is to be performed on behalf of the KTH Ship Dynamics Research Program. The background to the revision is the high interest in accurately capturing a ships dynamic response. The aim of the thesis it to explore the prospect of making use of the open source code *Nemoh* for modelling of added mass and damping in terms of modelling, computational efforts and ship motion prediction improvements. Both *SMS* and *Nemoh* is validated against reference data from commercial software´s and experimental studies. Furtherly, the thesis is written with the purpose to document and guide other users on how to operate and pre-process data for *Nemoh*. An approach with the aim to capture the speed-dependency of the hydrodynamic coefficients together with further potential development of *Nemoh* is addressed.

2. Theory behind modelling ship motion in waves

This chapter will give the reader a short introduction to the theory behind modelling of ship motions in waves.

2.1 Mathematical formulation

As described in (Lewis 1989), the starting point for modelling of ship motion in six degrees of freedom is Newton's second law,

$$\sum_{j=1}^{6} M_{ij}\ddot{\eta}_j = \mathbf{F}_i(t) \tag{2.1.1}$$

where $i, j = \{1,2,3\}$ are the translative- and $j, i = \{4,5,6\}$ are the rotative degrees of freedom as seen in Figure 1. Further denoted are the forces/moments $\boldsymbol{F_{ij}}$, mass/mass moments M_{ij} and translative/angular accelerations $\boldsymbol{\ddot{\eta}_j}$.

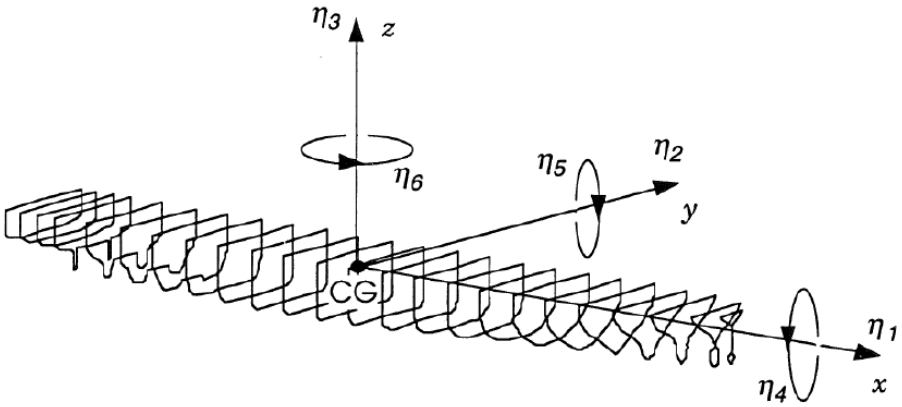

Figure 1:Translative degrees of freedom are, η_1 - surge, η_2 - sway, η_3 - heave and Rotative degrees of freedom are, η_4 - roll, η_5 - pitch and η_6 - yaw.

The forces on the left-hand side in Equation (2.1.1) may be expressed as the sum of the gravitational force F_{Gi} and fluid force F_{Hi} as stated in Equation (2.1.2).

$$\sum_{j=1}^{6} M_{ij}\ddot{\eta}_j = \mathbf{F}_i(t) = F_{Gi} + F_{Hi} \tag{2.1.2}$$

The gravitational forces are occurring due to the weight of the vessel applied at the centre of gravity. Since the mean gravitational forces cancel the mean buoyant forces, they are in this case a part of the hydrostatic fluid forces. The hydrostatic and hydrodynamic forces F_{HSi} & F_{HDi} may be expressed as the sum of the fluid forces that are acting on the ship as,

$$F_{Hi} = F_{HSi} + F_{HDi} \tag{2.1.3}$$

Both hydrostatic and hydrodynamic forces are obtained by integrating the fluid pressure over the underwater portion of the hull according to Equation (2.1.4) where P is the fluid pressure obtained from the *Bernoulli equation* (2.1.5) and n_i is the generalized unit normal to the hull surface. Pressure and gravitational forces are of greater magnitude compared to viscous forces in all degrees of freedom except roll. With the assumption of an inviscid, ideal fluid it's acceptable to apply *Bernoulli equation*.

$$F_{Hi} = \iint_S P n_i ds \tag{2.1.4}$$

$$P = -\frac{\rho U_0^2}{2} - \rho \frac{\partial \phi}{\partial t} + \frac{\rho}{2}\left(\Delta \phi^2\right) - \rho g z \tag{2.1.5}$$

The corresponding hydrodynamic and hydrostatic forces may be expressed as,

$$F_{HSi} = -\rho g \iint_S z n_i ds \tag{2.1.6}$$

$$F_{HDi} = -\rho \iint_S \left(\frac{U_0^2}{2} - \frac{\partial \phi}{\partial t} - \frac{1}{2}\left(\Delta \phi^2\right) \right) n_i ds \tag{2.1.7}$$

where U_0 denotes the forward speed of the ship. The hydrostatic forces from Equation (2.1.6) are combined with the gravitational forces F_{Gi} to give the net hydrostatic force F^*_{HSi}, which can be written in a more general matrix notation with respect to the six direction as,

$$F^*_{HSi} = F_{Gi} + F_{HSi} = -\sum_{i=1}^{6} C_{ij} \bar{\eta}_j e^{i\omega_e t} \tag{2.1.8}$$

where C_{ij} are the hydrostatic restoring forces, also known as the "spring coefficient", and the arbitrary motion η_j is replaced by $\bar{\eta}_j e^{i\omega_e t}$. The remaining hydrodynamic forces are calculated in accordance to Equation (2.1.7) where ϕ is the velocity potential for the fluid flow. In order to obtain the magnitude of the hydrodynamic forces, it's required to mathematically describe the fluid flow. When doing so, it's assumed to deal with an ideal fluid, i.e. incompressible, inviscid, irrotational and it follows that the fluid flow can be described in terms of a velocity potential ϕ as,

$$\phi = \left[-U_0 x + \phi_S(x, y, z) \right] + \left[\phi_I + \phi_D + \sum_{i=1}^{6} \phi_R \bar{\eta}_i \right] e^{i\omega_e t} \tag{2.1.9}$$

where the first term is called "steady part" and second term "unsteady part". The steady part of ϕ is due to the steady forward speed of the vessel and is not of interest when studying ships where the steady forward speed is zero. The unsteady part is however independent of time and only dependent on space variables. The potential ϕ_I is the incident wave potential i.e. the flow of the regular wave as if the hull was not there. The diffraction potential ϕ_D is the flow due to the presence of the body when it's motionless. The radiation potential ϕ_R is representing the waves generated by the body. The total unsteady part of the velocity potential can be described as a superposition of the incident potential ϕ_{I} and the solution of the diffracted and radiated potential ϕ_{D} and ϕ_{R} according to Equation (2.1.9).

The hydrodynamic forces that result from the incident and the diffracted waves are the exciting forces. The result from the radiation problem, for which is solved by oscillatory motions in 6 DOF, involve added mass and damping forces. With respect to the unsteady part of the velocity potential described in Equation (2.1.9), the unsteady hydrodynamic forces $\tilde{F}_{HDi}$, acting on the body consists of the excitation force F_{EXi} and the force due to forced motion F_{Ri}. The excitation force F_{EXi} is in turn described by the sum of the Froude-Krylov excitation force F_i^{FK} and the diffraction excitation force F_i^D as stated in Equation (2.1.10).

$$F_{EXi} = \{F_i^{FK} + F_I^{D}\} e^{i\omega_e t} \tag{2.1.10}$$

The Froude-Krylov excitation force is rather easily calculated since no hydrodynamic problem is to be solved, instead it's the result from a pressure integration over the body surface, as if the body were not present. The diffraction excitation force is obtained by solving Laplace equation (2.1.11) with the diffraction potential and respect to stated boundary conditions. Radiation forces results from the radiating waves due to the oscillating vessel as expressed in Equation (2.1.12), where A_{ij} and B_{ij} implies coupling between different degrees of freedom for the frequency varying added- water mass and damping coefficients. From a physical point of view, the added-mass coefficients represent the amount of fluid accelerated with the body. The damping coefficient represent the force component proportional to the velocity. In other words, it's related to the waves created by the motions of the vessel and the waves radiating from the vessel, dispersing energy from the oscillating movements.

$$\nabla \phi^2 = \frac{\partial^2 \phi}{\partial x^2} + \frac{\partial^2 \phi}{\partial y^2} + \frac{\partial^2 \phi}{\partial z^2} = 0 \tag{2.1.11}$$

$$F_{Ri} = \sum_{j=1}^{6} \left(\omega_e{}^2 A_{ij} - i\omega_e B_{ij} \right) \bar{\eta}_j e^{i\omega_e t} \tag{2.1.12}$$

The encounter frequency ω_e from Equation (2.1.12) is written as,

$$\omega_e = \omega - \frac{\omega^2}{g} U \cos\mu \tag{2.1.13}$$

where ω is the incident wave frequency, U is the ship forward speed and μ is the relative heading of the ship. To summarize the presented set of equations, the forces acting upon a submerged body that's influenced by the incident waves may be expressed as,

$$\begin{aligned} F_i &= F_{Gi} + F_{Hi} = F_{Gi} + (F_{HSi} + F_{HDi}) \\ &= (F_{Gi} + F_{HSi}) + (F_{EXi} + F_{Ri}) \\ &= F^*_{HSi} + F_{EXi} + F_{Ri} \end{aligned} \tag{2.1.14}$$

combining the stated forces with corresponding expressions presented in Equation (2.1.8) & (2.1.12), the linearized equations of motions to be yield is expressed in Equation (2.1.15).

$$\sum_{j=1}^{6} \eta_j \left[-\omega^2 \left(M_{ij} + A_{ij} \right) + i\omega B_{ij} + C_{ij} \right] = F_i^{FK} + F_i^{D} \tag{2.1.15}$$

There exist different approaches when it comes to determining the coefficients and excitation forces. One of these approaches is the implementation of Lewis-forms according to de Jong (1973) which is also implemented to the "strip-method" simulation code *SMS*. Another approach is to implement Boundary Element Methods (BEM), also known as panel methods, which is applied in *Nemoh*. The following sections describe both these methods.

Once the hydrodynamic coefficients have been determined, the linearized equation of motion can easily be solved in the frequency domain from Equation (2.1.16).

$$\eta_j = \frac{F_{ex}}{-\omega^2\left(M_{ij} + A_{ij}\right) + i\omega B_{ij} + C_{ij}} \tag{2.1.16}$$

2.2 Non-linear models

The friction between hull and water, i.e. the viscous effects, is important to consider when modelling a ships motion in waves (Rosén 2011). The two main degrees of freedom where viscous effects are of importance are surge but mainly roll. A simplified approach for capturing the viscous effects in surge is to estimate the total drag due to the fluid flow on a plate with the same dimensions as the submerged part of the hull. In the case of roll it's feasible to capture the viscous effects from experimental roll decay tests or non-linear simulation models. This is of great importance in the case of roll since viscous effects are non-linear and significantly larger in magnitude compared to pressure and gravitational forces, as earlier addressed.

Non-linear effects can also be significant in the Froude-Krylov and restoring forces for hulls with flared bow and aft. Such effects are particularly important to take into consideration for example when modelling parametric rolling and loss of stability. The modelling here has to be made in the time-domain to enable consideration of the momentary interaction between the wave surface geometry and hull geometry and the related non-linearities.

3. Strip Methods

A good estimate of hydrodynamic forces is obtained when applying strip theory to slender bodies. With the theory, the submerged part of the ship is divided into a finite number of strips. By applying a two-dimensional approach it's assumed that the variation of the fluid flow in the cross-directional plane is much larger than the variation in the longitudinal direction. The three-dimensional coefficients for added mass, damping and the wave excitation forces can be obtained by integrating the two-dimensional coefficients for each strip over the length of the vessel. The fundamental idea behind strip theory is therefore to reduce the three-dimensional hydrodynamical problem to a series of two-dimensional problem which are easier to solve. This is very briefly described below, where the starting point is Equation (2.1.12). The added mass and damping coefficients can be defined by a complex force coefficient as,

$$\begin{aligned} T_{ij} &= \omega_e{}^2 A_{ij} - i\omega_e B_{ij} \\ &= \rho \iint n_i \left(i\omega_e - U_0 \frac{\partial}{\partial x} \right) \phi_k ds \end{aligned} \tag{3.1.1}$$

In order to solve T_{ij}, one need to solve a boundary value problem for the radiation potential ϕ_k and then integrating over the hull surface. The boundary value problems lead to two separate components of the radiation potential and in combination with the slender body approach, it allows T_{ij} from Equation (3.1.1) to be expressed in terms of two-dimensional sections as,

$$\begin{aligned} T_{ij}{}^0 &= -\rho i\omega_e \int_L \int_{C_x} n_i \phi_k{}^0 dl dx \\ \{T_{ij} &= T_{ij}{}^0 \ldots i, j = 1,2 \ldots 4\} \end{aligned} \tag{3.1.2}$$

where dl denotes the integral around the section contour C_x and dx denotes the integral along the ship length L. With further approximations regarding the boundary conditions and the two-dimensional Laplace equation it follows that ϕ_k^0 and line integrals from Equation (3.1.2) may be the solution to a series of two-dimensional problems at various sections along the length of the ship. The 2-D sectional coefficients for added mass and damping may be defined according to Equation (3.1.3) - (3.1.5) where N_i & ψ_i denotes the two-dimensional normal and velocity potential (Lewis 1989).

$$\begin{aligned} \omega_e a_{ii} - i\omega_e b_{ii} &= -\rho i\omega_e \int_{Cx} N_i \Psi_i \\ i &= 1,2..4 \end{aligned} \tag{3.1.3}$$

$$\begin{aligned} \omega_e a_{13} - i\omega_e b_{13} &= \omega_e a_{31} - i\omega_e b_{31} \\ &= -\rho i\omega_e \int_{Cx} N_1 \Psi_3 \end{aligned} \tag{3.1.4}$$

$$\begin{aligned} \omega_e a_{24} - i\omega_e b_{24} &= \omega_e a_{42} - i\omega_e b_{42} \\ &= -\rho i\omega_e \int_{Cx} N_2 \Psi_4 \end{aligned} \tag{3.1.5}$$

By using the relations listed above, it's possible to express the vertical and horizontal modes of the added mass and damping coefficients for a ship with port/starboard symmetry as listed and derived from Appendix D in (Palmquist and Hua 1995).

The excitation force F_{EXi} obtained with Strip-Theory is as stated in Equation (2.1.10), the sum of the Froude-Krylov excitation force F_i^{FK} and the diffraction excitation force F_i^D. The sectional Froude-Krylov exciting force amplitudes $f_i(x)$ and sectional diffraction exciting force amplitudes $h_i(x)$ is defined according to Equation (3.1.6)-(3.1.7).

$$f_j(x) = \rho g \bar{\xi} \int_{C_x} N_j e^{-iky\sin\mu} e^{kz} dl \ldots j = 1,2,3,4 \tag{3.1.6}$$

$$h_j(x) = \rho \bar{\xi} \omega_0 \int_{C_x} (iN_3 + N_1\cos\mu + N_2\sin\mu) e^{-iky\sin\mu} e^{kz} \psi_j(y,z) dl \ldots j = 1,2,3,4 \tag{3.1.7}$$

The corresponding three-dimensional forces may then be described as stated in (Lewis 1989) as,

$$F^I{}_j = \int_L e^{-iky\cos\mu} f_j(x) dx \ldots j = 1,2,3,4 \tag{3.1.8}$$

$$F^I{}_5 = -\int_L e^{-iky\cos\mu} x f_3(x) dx \tag{3.1.9}$$

$$F^I{}_6 = \int_L e^{-iky\cos\mu} x f_2(x) dx \tag{3.1.10}$$

$$F^D{}_j = \int_L e^{-iky\cos\mu} h_j(x) dx \ldots j = 1,2,3,4 \tag{3.1.11}$$

$$F^D{}_5 = -\int_L e^{-iky\cos\mu} (x + \frac{U_0}{i\omega_e}) h_3(x) dx \tag{3.1.12}$$

$$F^D{}_6 = \int_L e^{-iky\cos\mu} (x + \frac{U_0}{i\omega_e}) h_2(x) dx \tag{3.1.13}$$

Lewis-form is a method for calculating the potential flow around two-dimensional sections using a conformal mapping technique. The technique is used for deriving the velocity potential for an arbitrary cross-section by mapping a more convenient circular section in another complex plane. The hydrodynamic problems for the ship can then be solved directly with the coefficients of the mapping function.

Lewis-forms is one of three existing computing techniques for solving the two-dimensional sectional hydrodynamic quantities expressed in Equation (3.1.3)-(3.1.5). The three methods disregard the viscous effect and the main difference is how the velocity potential is solved for an oscillating cylinder in modes of sway, heave and roll. The background to this is when Ursell (1949) used a multipole method in order to satisfy the Laplace equation at the free-surface boundary conditions for a heaving circular cylinder. These results could later be used with conformal mapping in order to yield solutions for Lewis-form which resemble ship sections. The Lewis two-parameter conformal mapping formula – see also Figure 2 - is given by,

$$z = M_s(\xi + a_1\xi^{-1} + a_3\xi^{-3}) \tag{3.1.14}$$

with:

- a_1, a_3 as Lewis coefficients,
- M_s as the scale factor,
- $\xi = ie^{\alpha}e^{-i\theta}$, where α denotes the angle of the section edge (not included in Figure 2).
- $z = x + iy$.

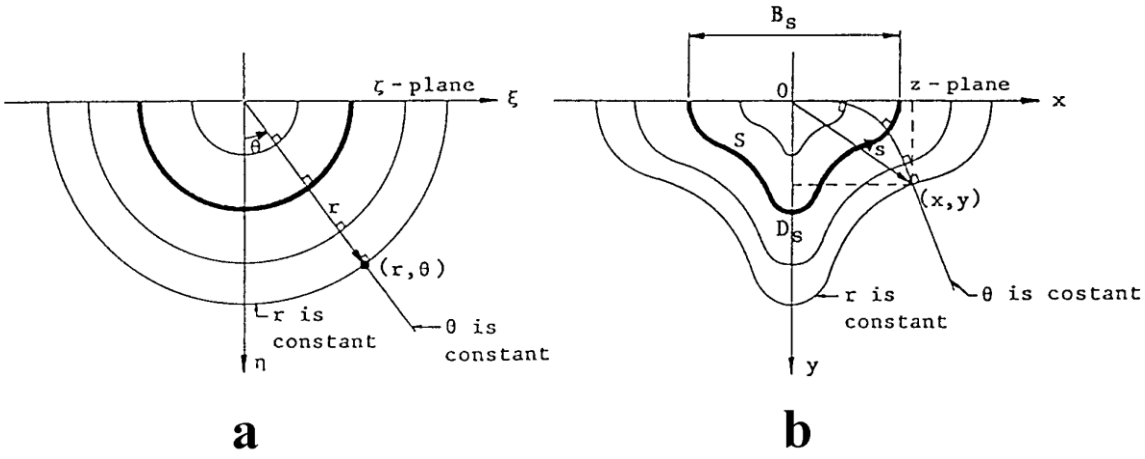

Figure 2: Mapping relation between two planes (Journée and Adegeest 2003)

Starting with a conventional hull-shape as presented in Figure 2 *b)*, it's possible to derive the Lewis coefficients in such a manner that the sectional breadth, draught and area are identical between the approximated cross section *a)* and of the actual hull-geometry *b)*. Further in-depth theory is treated in the *Theoretical Manual of "Seaway",* (Journée and Adegeest 2003).

The advantages of utilizing Lewis-form is the low computational effort that is required to solve the velocity potential and obtaining the hydrodynamic quantities. The disadvantages are however the ability to approximate unconventional ships' shape by a continuous function. The complete hydrodynamic characteristics are not obtained for ships with close to quadratic midsections or for ships with a high beam to draft ratio. Other complications are sharp corners and submerged parts such as bulbs. In consequence, numerous studies have been published, presenting extended- and close fit conformal mapping techniques considering higher order mapping parameters.

4. Panel methods

Conformal mapping techniques have the disadvantages of not capturing a hull's full characteristics by a continuous function, in consequence are panel methods alternatively used. With Panel methods, source technique is used to analyse linear wave-induced loads on large-volume structures. A source is strictly defined as a point from which fluid is imagined to flow out uniformly in all directions (O. Faltinsen 1990). Strip theory are commonly used with a two-dimensional panel method. The approach, where strips of the ship are defined by a set of two-dimensional panels, are seen as more accurate than conformal mapping techniques. Another approach is to distribute three-dimensional panels over the whole surface of the ship, further seen as an accurate but time demanding approach.

Hess and Smith (1964) pioneered the development of Panel methods in aeronautics and laid the foundation for its applications to ship flows. They found that sources could be distributed over the surface if the body is approximated by a large number of small plane elements, also known as quadrilateral panels. These elements consist of four nodes, describing the corners of the panel. Two diagonal vectors define the normal vector from the cross-product and the centre of the panel is defined from averaging the coordinates of the four nodes. The plane of the panel is considered from the centre point and the normal (Bertram 2000).

The theory for solution of the velocity potential and radiation and diffraction forces in the frequency domain is very well described in (McTaggart 2002). The diffracted or radiated velocity potential at a location in the fluid domain is described as,

$$\phi(\vec{x}) = \frac{1}{4\pi}\int_{S_b} G(\vec{x},\vec{x}_S)\sigma(\vec{x}_S)dS \tag{4.1.1}$$

where,

- $\vec{x}$ is the source location on the surface of the ship
- S_b denotes the mean wetted surface of the ship
- $G(\vec{x}, \vec{x}_s)$ is the Green function describing the flow at that location due to a source of unit strength at $\vec{x}_S$
- $\sigma(\vec{x}_s)$ describes the strength of the source at $\vec{x}_S$

The Green function satisfies all the boundary conditions stated with the exception of the normal velocity boundary condition expressed on the hull surface as,

$$\frac{\partial\phi(\vec{x})}{\partial n} = v_n(\vec{x})\ldots on\ldots S_b \tag{4.1.2}$$

where $v_n(\vec{x})$ is the normal velocity of the flow on the hull surface. With respect to previously stated boundary condition, the source strengths are solved by satisfying the equation,

$$-\frac{1}{2}\sigma(\vec{x}_S) + \frac{1}{4\pi}\int_{S_b}\frac{\partial G(\vec{x},\vec{x}_S)}{\partial n_{\vec{x}}}\sigma(\vec{x}_S)dS = v_n(\vec{x})\ldots on\ldots S_b \tag{4.1.3}$$

The hull boundary condition for radiation and diffraction potentials are stated in Equation (4.1.4) and (4.1.5).

$$\frac{\partial\phi_K(\vec{x})}{\partial n} = i\omega_e n_k\ldots on\ldots S_b \tag{4.1.4}$$

$$\frac{\partial \phi_D(\vec{x})}{\partial n} = -\frac{\partial \phi_I(\vec{x})}{\partial n} \ldots on \ldots S_b \tag{4.1.5}$$

With a panelled hull, the solutions of the source strengths are solved by satisfying the discretized form of Equation (4.1.3) with,

$$\{\partial \phi / \partial n\} = \left[D \right] \{\sigma\} \tag{4.1.6}$$

where the first term, $[D]$, denotes the velocity potential influence matrix given by,

$$D_{jk} = -\delta_{jk} \frac{1}{2} + \frac{1}{4\pi} \int_{S_k} \frac{\partial G(\vec{x}_j, \vec{x}_S)}{\partial n_{\vec{x}_j}} \sigma(\vec{x}_S) \tag{4.1.7}$$

where $\delta_{jk}$is the Kroenecker delta function and S_k denotes the surface with respect to panel *k* and mode *j*. After determining source strengths $\{\sigma\}$, the potentials on the hull surface are given as,

$$\left\{\phi\right\} = [E] \left\{\sigma\right\} \tag{4.1.8}$$

where $[E]$ is the velocity potential influence matrix described in Equation (4.1.9).

$$E_{jk=} \frac{1}{4\pi} \int_{S_k} \partial G(\vec{x}_j, \vec{x}_S) dS \tag{4.1.9}$$

With obtained potentials, the forces can be calculated with Bernoulli (2.1.5) and from that, the added-mass and damping coefficients may be determined.

With presented mathematical theories there is a need to address practical complications caused by the advent of computer assistant numerical methods, one of which is the case of *irregular frequencies*. When solving for the strength of the sources with Greens formula, there might be inconsistent results i.e., non-finite solutions to the integral equation for corresponding *irregular frequencies*. Faltinsen (1990) explains the phenomena to occur since the *irregular frequencies* represent eigenfrequencies for a fictious fluid motion inside the body with the same free-surface conditions outside the body. This is not a physical phenomenon, instead the impact is in the form of un-consistent amplitude peaks.

Panel methods are restricted to bodies where the oscillations amplitudes of the fluid and the body is small in relation to the cross-sectional dimension of the bodies. Panel method cannot predict rolling motion of a ship for frequencies close to the roll resonance frequency since damping is predicted with regard to radiation of surface waves (O. Faltinsen 1990).

5. Nemoh

The open source code Nemoh is a numerical solver for computation of first order hydrodynamic coefficients such as added mass, radiation, damping and excitation forces in the frequency domain (Babarit and Delhommeau 2015). The code has been developed for over 30 years at École Centrale de Nantes in France and was released in open source in January 2014. Nemoh is based on linear free surface potential flow theory with assumptions of an inviscid fluid and an incompressible and irrotational flow. Green´s second identity and the appropriate Green function is applied. The resulting linear Boundary Value Problem (BVP) for the free surface flow around a body is of first order with assumptions of small motions around mean position and linearized free surface equations. In order to solve the linear BVP, Panel methods are applied in Nemoh. Nemoh can both be operated in Matlab and in command line.

Nemoh is composed of three different sets of programs for which are intended to run in sequent order listed as,

- *preProcessor,* reads and prepare the mesh and calculation cases with stated body conditions
- *solver*, solves the linear BVP with potential theory for stated body condition and calculates hydrodynamic coefficients
- *postProcessor*, processes the results and may be used for calculating RAOs and plot free surface wave elevation.

A Matlab wrapper is provided with the programs in order to define and process geometries and results in a more user-friendly environment. The mesh is composed of flat quadrangular panels with four nodes, oriented counter-clockwise, as seen from the fluid domain looking into the body. Two Meshing tools are provided in order to define a geometry for the *preProcessor*. One of which are the "*Mesh.m*" tool, used for bodies with a symmetry about the x0z-plane, where only half of the submerged body is to be described. The characteristics of the panels have to be defined in a four-dimensional matrix X as,

$$X(Body, Panel, Node, Coordinate) \tag{5.1.1}$$

i.e. the current body described by panels with nodes and corresponding 3-dimensional coordinates. The coordinates of first Panel would therefore be,

$$X(1,1,:,:) = [(x_1, y_1, z_1); \ldots\ldots (x_4, y_4, z_4)] \tag{5.1.2}$$

Other inputs required for the "*Mesh.m*" tool is,

- $nBodies$, number of bodies
- n is number of panels
- tX is translation of coordinate system
- CG is the position of centre of gravity
- $nfobj$ is the resolution of panels.

The mesh tool stores information regarding the geometry and its characteristics, such as hydrostatic stiffness matrix "*KH*" and mass- and inertia matrix "*M*", which will be of importance when running Nemoh. It is however of great importance to look over the mass- and inertia matrix "*M*" since the "*Mesh.m*" tool estimates the centre of mass and corresponding inertia matrix independent from the defined centre of gravity. In the current version of Nemoh, one should discard the inertia matrix that is provided by the "*Mesh.m*" tool and instead define it manually with respect to the actual centre of

gravity. The command "$nfobj$ "in "Mesh.m" is of great interest since a hull geometry of low resolution easily could turn into a high-resolution geometry. Figure 3 shows a hull defined accordingly to the input for "*Mesh.m*" where the arrows represent the normal vector for the corresponding panel. The right-handed equilibrium axis system *Oxy* has its origin defined in Centre of Gravity and z-axis origin is defined at the water-surface. The z-axis is defined positive upwards and the ship will be advancing in the positive direction of the x axis.

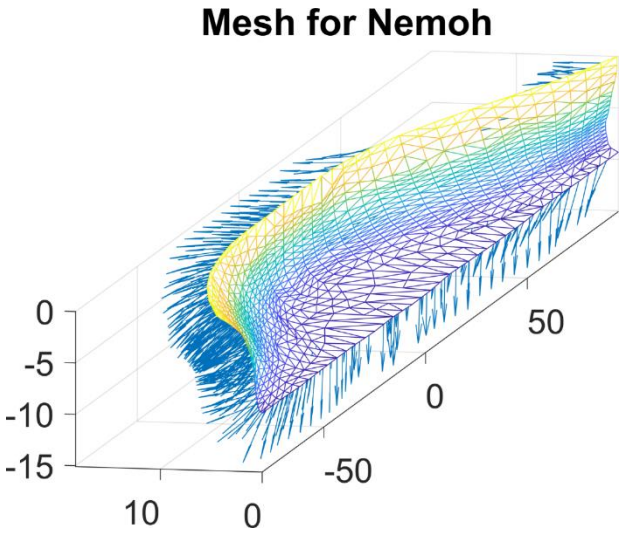

Figure 3: A hull defined accordingly to input for "Mesh.m"

Once Nemoh is ran, the *postProcessor* has stored the relevant quantities and provided a framework to make relevant calculations. Some of which are data on calculated added mass and damping coefficients, radiation forces, excitation forces and corresponding RAOs. Nemoh is also capable of postprocessing free surface elevation and far field coefficients and supports visualization in Tecplot for mesh and forces such as Froude-Krylov. Further information regarding the architecture and the tool created for geometry conversions are presented in Appendix 1.

Nemoh is restricted to calculate linear hydrodynamic coefficients in waves at zero Froude numbers i.e. zero forward speed. The viscous effects are not taken into account in Nemoh and its therefore required to compensate the damping coefficient in roll with data from a Roll-Decay test or some other method such as Ikea or CFD in order to compute the RAOs in roll. *Nemoh* is not capable of removing irregular frequencies, potential actions for handling this is discussed in Chapter 7.3.

6. Validation of Nemoh

There are not many published papers where three-dimensional hydrodynamic coefficients have been validated between different software's with respect to zero Froude numbers. This chapter focus on identifying, collecting and presenting papers that will be utilized as a basis in the validation process. Transferfunctions from Nemoh and SMS are compared to other theories and software's such as *Wamit* and *ShipMo* in Chapter 6.4-6.6. Only result from *Nemoh* and *SMS* were computed, the rest of the presented results in Chapter 6.4-6.6 are reference data from the referenced authors. All results presented in Chapter 6 are calculated with zero forward speed. In order to determine a convenient number of panels for the computations of *Nemoh*, a convergence analysis is performed and presented in Chapter 6.1 with the intention to ensure results of high accuracy.

6.1 Convergence Analysis & Computational Effort

A convergence analysis is performed in *Nemoh* for hydrodynamic coefficients of a barge and transfer functions in heave for three different ships, the computational time between *SMS* and *Nemoh* is also identified. The three ships for which are also used in the validation process of *Nemoh* are a "6750-TEU", "S-175" and a "Series-60" ship.

The result from a convergence analysis on a Box, initially described by 4 panels, is presented in Figure 4. It's clearly distinguishable from the figure that *Nemoh* is converging quickly to the result obtained at a panel resolution of 1800 for all four cases.

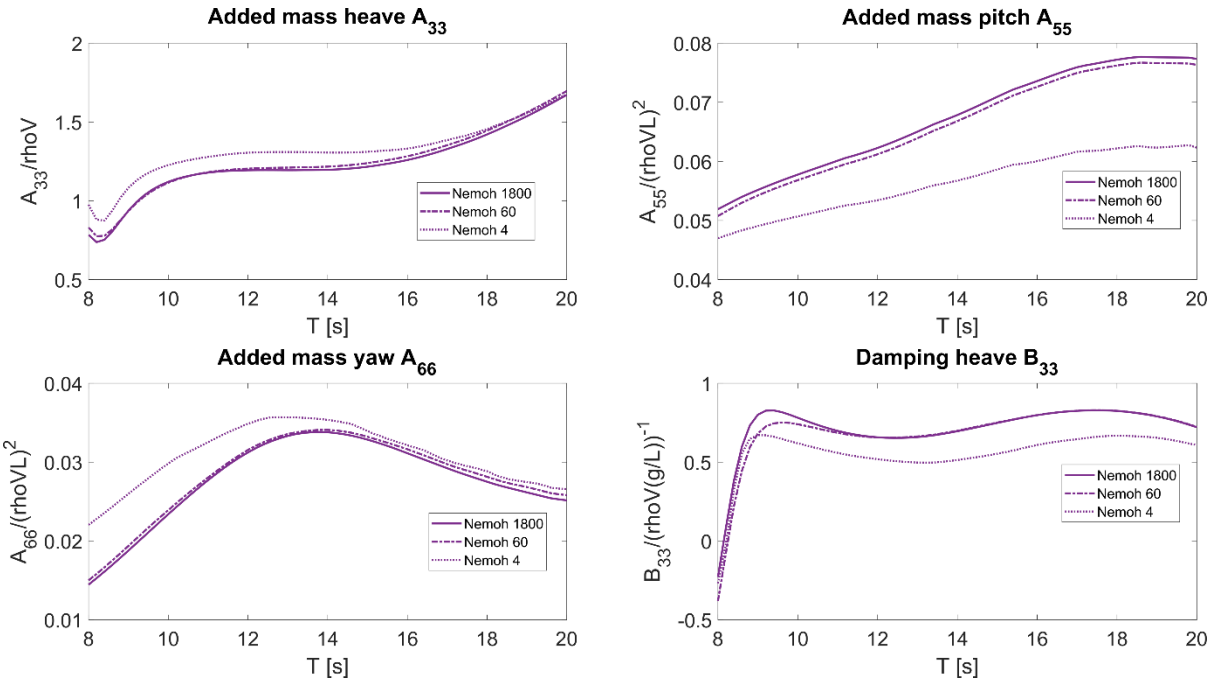

Figure 4: Convergence analysis with respect to hydrodynamic coefficients for a box travelling at Zero Froude Number at infinite depth

RAOs in Heave were expressed according to Equation (2.1.16) with a frequency vector of 50 components at four different panel resolutions. The decision of loading case, heading and frequency vector is consistent with the result presented in Chapter 6.4-6.6. The heading is therefore set to head seas except for "S-175" which is computed in quartering beam seas. The choice of having such a high resolution in frequency is set with respect to the input from *SMS*, with intention of comparing computational efforts. The result from the convergence analysis is presented in Figure 5.

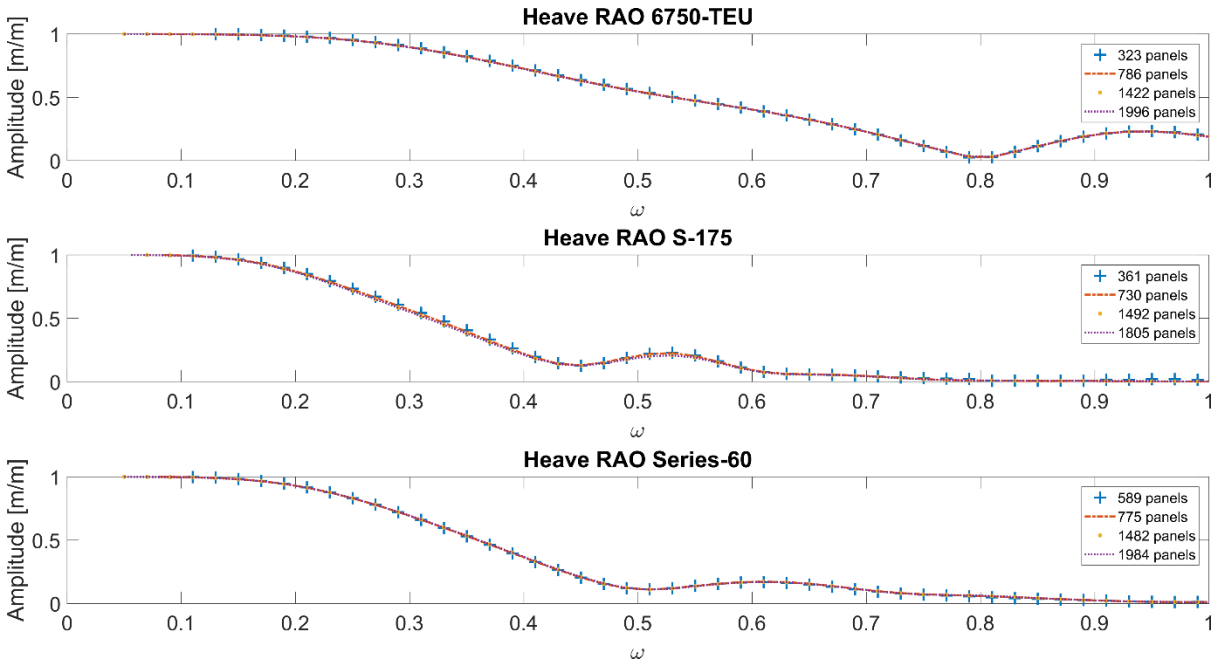

Figure 5: Convergence analysis in Heave for three different types of ships travelling at Zero Froude Number at infinite depth.

One may clearly distinguish that *Nemoh* converges as good as instantly to the result obtained at higher panel resolutions.

The presented convergence analysis verifies that a panel resolution of 800, which has been used in Chapter 6.2-6.6, is more than sufficient to ensure result of high accuracy. The result does also ensure that a resolution of 800 panels is sufficient when running similar ship geometries in *Nemoh*.

The computations have been performed with an Asus-laptop using, Intel(R) Core(TM) i5-6200U CPU @ 2.30GHz, 2400 Mhz, 2 cores, 4 logical processors and 12 GB of RAM. Using only one core, the actual speed between runs were measured to 2.72 GHz. The run time in *Nemoh* and *SMS* with respect to grid size and ship is presented in To further clarify, the difference in runtime between RAOs and hydrodynamic coefficients are basically the same in *Nemoh* since RAOs are expressed in terms of the hydrodynamic coefficients according to Equation (2.1.16).

Table 1: Computational effort between Nemoh and SMS with respect to grid size and a frequency vector of 50 components

6750-TEU		**S-175**		**Series-60**	
Panel resolution	Run time *Nemoh*	Panel resolution	Run time *Nemoh*	Panel resolution	Run time *Nemoh*
323	50.2 sec	361	60.0 sec	589	205.8 sec
786	320.5 sec	730	265.0 sec	775	360.4 sec
1422	1420.7 sec	1492	1475.7 sec	1482	1504.0 sec
1996	3018.5 sec	1805	2423 sec	1984	3327.0 sec
Sections/ Points total	Run time *SMS*	Sections/ Points total	Run time *SMS*	Sections/ Points total	Run time *SMS*
18/1206	0.92 sec	20/1220	0.93 sec	23/1081	0.94 sec

The computational effort presented between *SMS* and *Nemoh* clearly shows how computational efficient Strip Method is. Even with the lowest panel resolution obtainable in *Nemoh* the run time is significantly higher in comparison to *SMS*. From the results presented in Figure 4, Figure 5 and Table 1 it may be concluded that a lower panel resolution is in this case a suitable choice considering both computational efficiency and accuracy.

6.2 Hydrodynamic coefficients for a Barge

The reference data used is in the form of experimental and numerical result of the added mass coefficient in heave, pitch and yaw and the damping coefficient in heave simulated for a barge with dimensions L x B x T equal to 90x90x20m at infinite depth. The comparison is presented in Figure 6-Figure 9. The two models used in the report of Faltinsen and Michelsen (1975) are referred to as, "3D Source", a three-dimensional source technique as introduced in Chapter 4 and "Strip", a program based on strip theory as introduced in Chapter 3. The results presented in the report works as reference data when it comes to the validation of *Nemoh* since the three-dimensional source technique is said to be "adequate" according to Faltinsen and Michelsen (1975) when simulating the dynamic response of a barge.

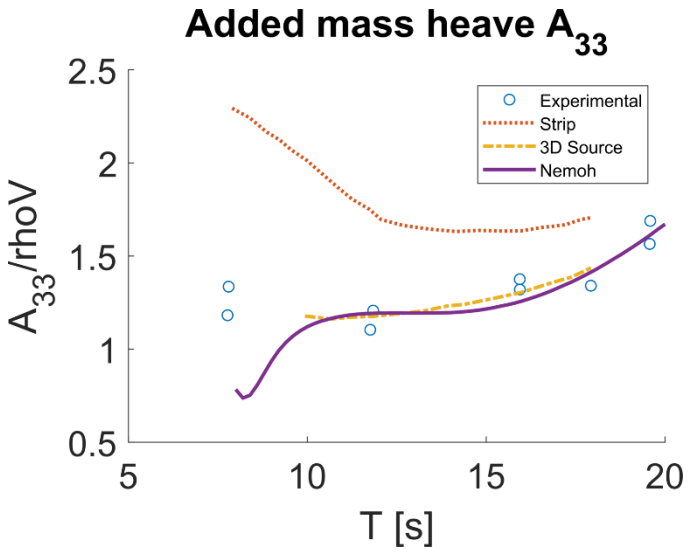

Figure 6: Added mass in Heave for Barge at Zero forward speed

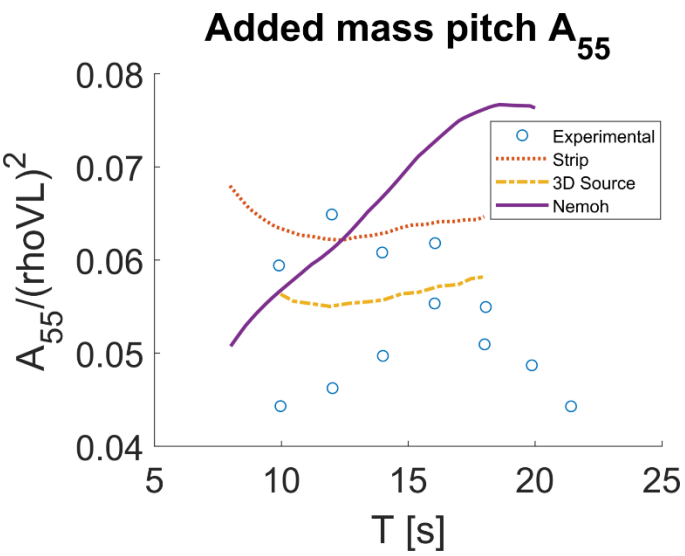

Figure 7: Added mass in Pitch for Barge at Zero forward speed

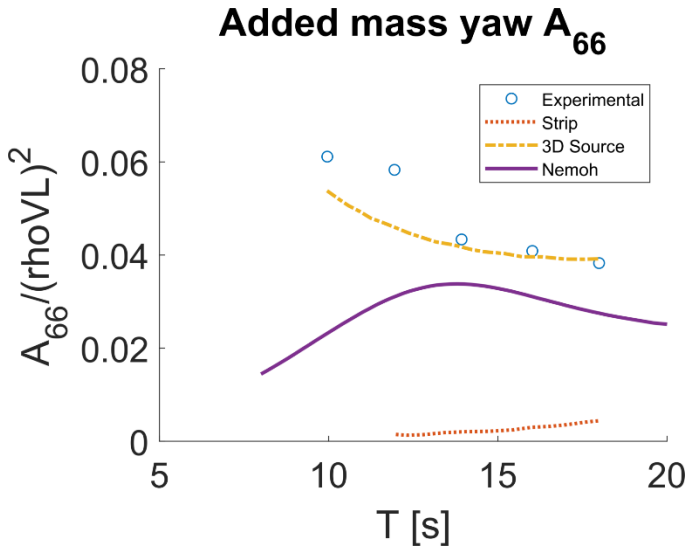

Figure 8: Added mass in Yaw for Barge at Zero forward speed

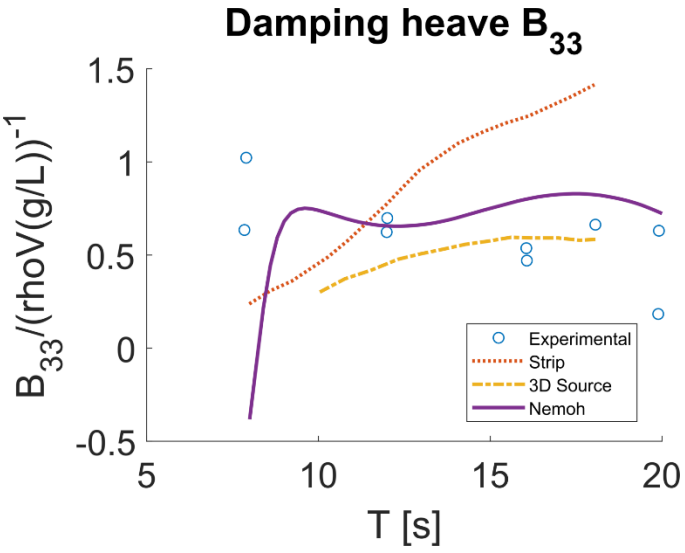

Figure 9: Damping in Heave for Barge at Zero forward speed

Result from *Nemoh* shows very good agreement with the result from experimental setups and "3D Source" studies for added mass and damping in heave. When it comes to the result for added mass in pitch and yaw there are some factors that might have caused the larger difference between Nemoh and the computed 3D source data. One is that the hull geometry for the Barge is defined without the

aft and bow sides when calculating the hydrodynamic coefficients in Nemoh. It's clearly presented that the result from two-dimensional Strip Theory isn't adequate with a geometry of a barge compared to experimental and three-dimensional result, especially in the case of yaw and heave.

6.3 Hydrodynamic coefficients for a Box

The geometry utilized in *Nemoh* in this section has the dimensions L x B x T equal to 2x8x40m and calculated at infinite depth. Sectional added mass and damping coefficients in sway and heave for a box with Beam to Draught ratio of 4 has been published in Lewis (1989) and is here used as reference data. The sectional coefficients have here been integrated along the length of the ship in order to

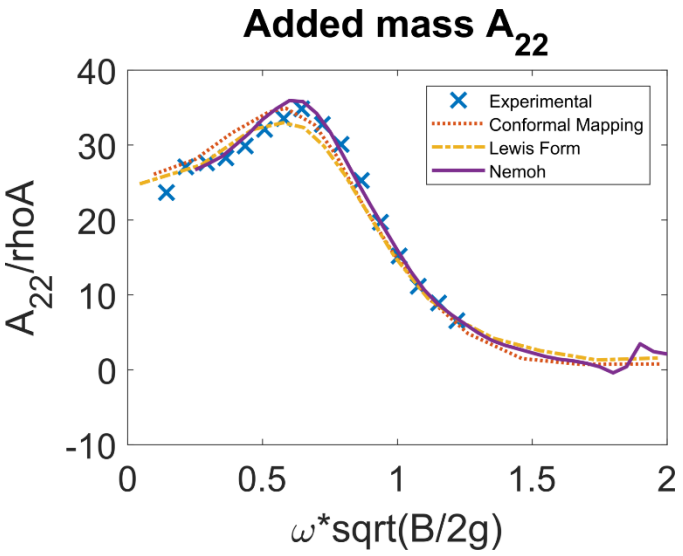

Figure 10: Added mass in Sway for Box at Zero forward speed

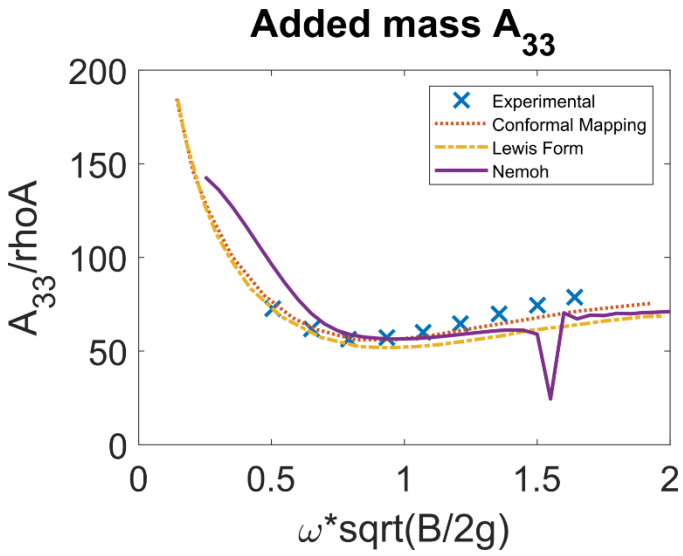

Figure 11: Added mass in Heave for Box at Zero forward speed

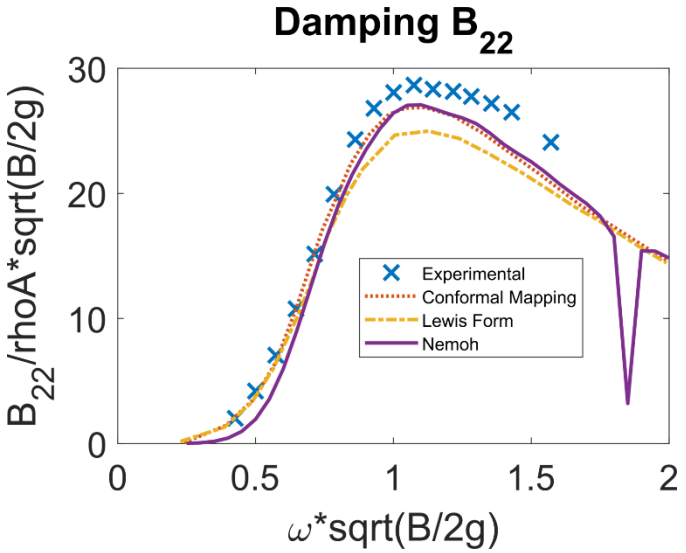

Figure 12: Damping in Sway for Box at Zero forward speed

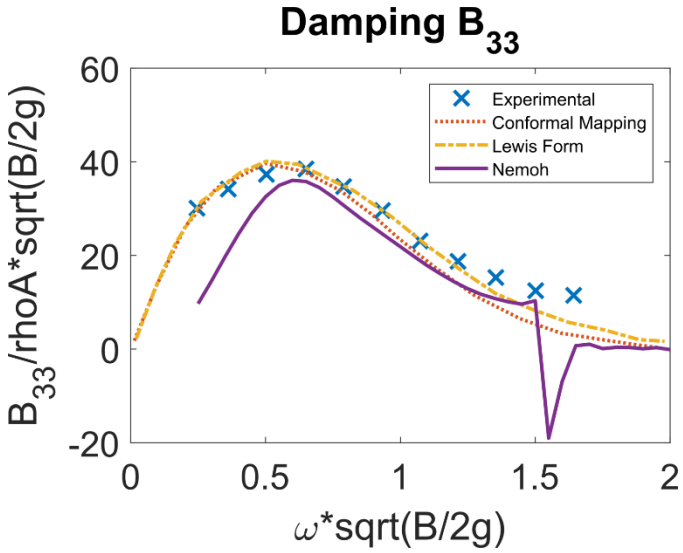

Figure 13: Damping in Heave for Box at Zero forward speed

generate three-dimensional coefficients for comparison with *Nemoh*. The individual points in Figure 10 - Figure 13 present experimental results while the dashed curve indicates result from conformal mapping, point dash indicates Lewis forms as presented in Chapter 3 and the solid curve is the result from *Nemoh*. The main difference between Conformal mapping and Lewis is that conformal mapping utilizes more parameters and is therefore seen as more accurate.

As mentioned in Lewis (1989) and as one may distinguish in Figure 11 is that the multi-parameter conformal mapping technique complies better with the experimental results, and so does *Nemoh*. At frequencies corresponding to a period of 2.7 or higher, results from *Nemoh* shows the case of "irregular frequencies" and should be disregarded, as mentioned in Chapter 4.

6.4 Response Amplitude Operators for a 6750-TEU Containership

The hull-geometry for the 6750-TEU containership used in this section is presented in Figure 14 and corresponding dimensions in Table 2. Response Amplitude Operators for heave and pitch from *Nemoh* and *SMS* have been compared against a benchmark study for a 6750-TEU containership with zero forward speed. The benchmark test focus on the performance of seakeeping analysis codes as a part of the 2nd ITTC-ISSC joint workshop in 2014. A total of eleven institutes participated in the benchmark test with seventeen analysis codes (Kim and Kim 2016).

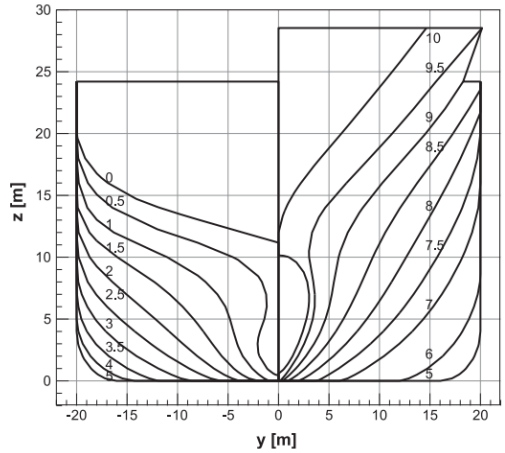

Figure 14: Body Plan of the 6750-TEU Containership

Table 2: Principal dimensions of the 6750-TEU Container ship

LOA (m)	300.891
LBP (m)	286.6
Breadth (m)	40
Height (m)	24.2
Draft (m)	11.98
Displacement (ton)	85,562.7
KM (m)	18.662
GM (m)	2.1
LCG from AP (m)	138.395
Natural Period of Roll (s)	20.5

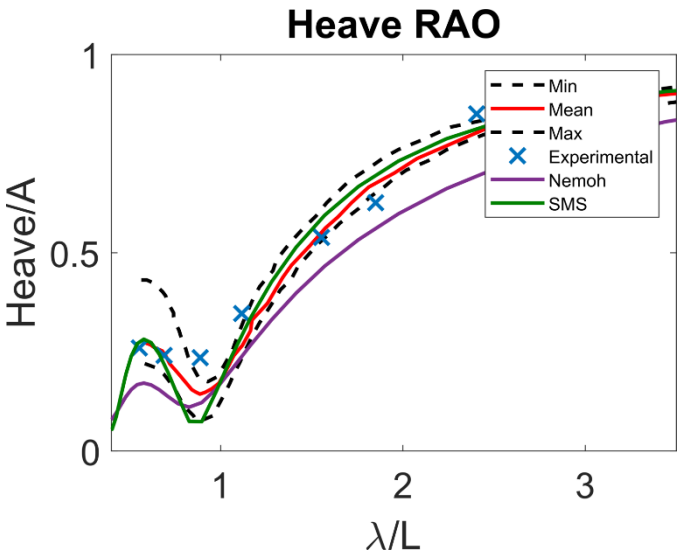

Figure 15: Heave RAO for a 6750-TEU Containership with zero forward speed in head seas

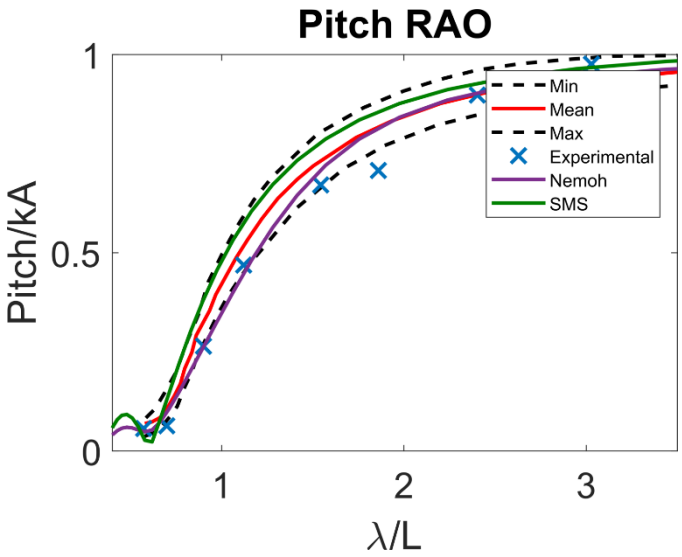

Figure 16: Pitch RAO for a 6750-TEU Containership with zero forward speed in head seas

RAOs from both Nemoh and SMS have been generated with regard to the loading case in Table 2 (Kim and Kim 2016). The 17 analysis codes utilize methods such as 3D BEM, Strip Method, Panel-Free Method, IRF and Ranse. An average of computational results is presented with corresponding minimum and maximum values in Figure 15 & Figure 16.

The result obtained from *SMS* show good agreement with the benchmark tests for both heave and pitch. *Nemoh* shows good agreement for Pitch while the result for Heave is significantly different in amplitude.

6.5 Response Amplitude Operators for a S-175 Containership

RAOs are computed for all degrees of freedom for the containership S-175 in quartering beam seas for zero forward speed at infinite depth. The main dimensions and Body plan are presented in Table 4 and Figure 17. A Body-Exact Strip Theory Approach to ship motion computations is introduced in Bandyk (2009) and is validated against *ShipMo* and a linear strip theory variant derived by Ogilvie and Tuck (1969). The Body-Exact Strip Theory Approach is based on a combination of a body-nonlinear time-domain approach coupled with nonlinear equations of motion, shortly introduced in Chapter 2.2. The two-dimensional strip theory software, *ShipMo*, utilizes potential theory and relies on the slenderness of the hull form and on the linearity of the hydrodynamic forces as introduced in Chapter 3.

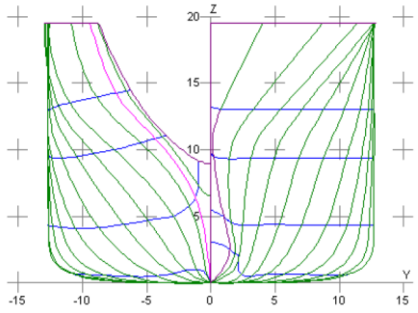

Figure 17: Body Plan of the S-175 Containership

Table 3: Dimensions of the S-175 Containership

LPP (m)	175
Breadth (m)	25.4
Draught (m)	9.5
Block-coefficient	0.57

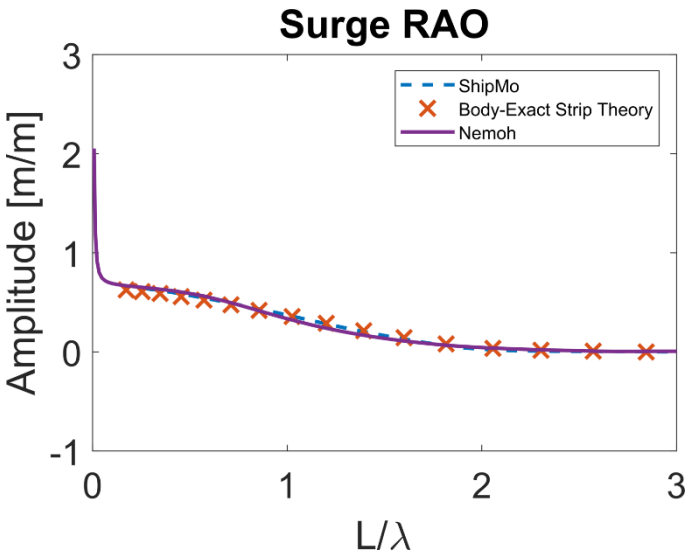

Figure 18: Surge RAO for S-175 Containership with zero forward speed in quartering beam seas

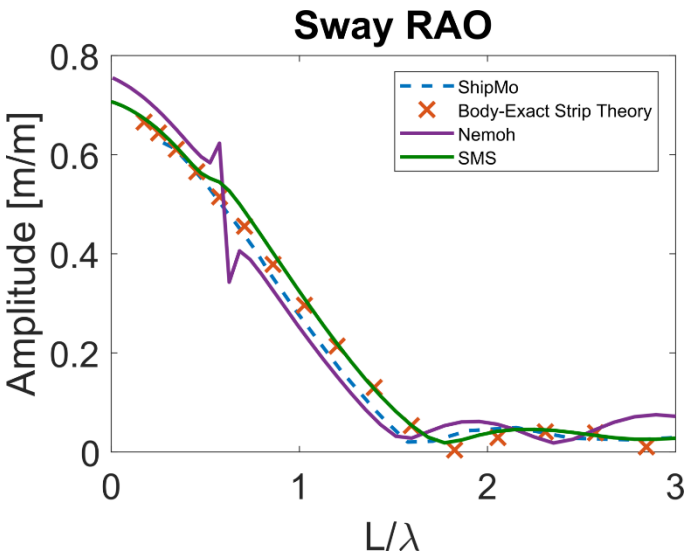

Figure 19: Sway RAO for S-175 Containership with zero forward speed in quartering beam seas

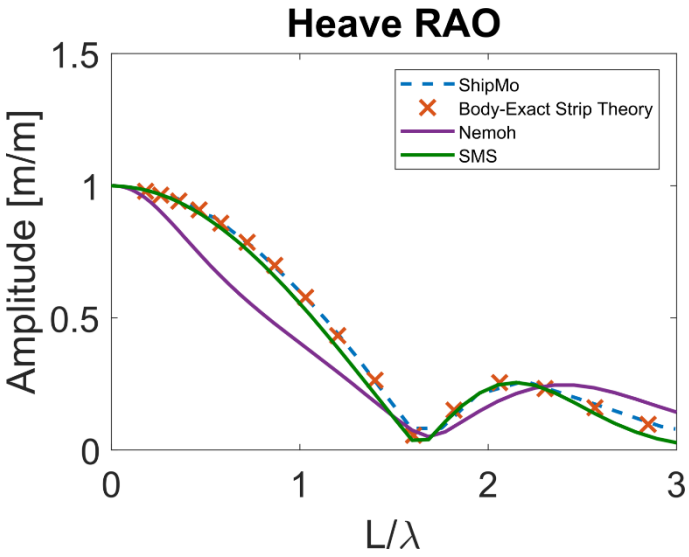

Figure 20: Heave RAO for S-175 Containership with zero forward speed in quartering beam seas

Since the Body-Exact Strip Theory approach is mentioned to be an accurate and robust tool (Bandyk 2009), it's used as reference data in the validation process of *Nemoh*, together with *SMS*. The result from the comparison is presented in Figure 18-Figure 20. *Nemoh* shows very good agreement to the reference data in the case of Surge and Sway.

When analysing the results from the rotative degrees of freedom, it was found that the amplitudes were deviating much larger than the RAOs calculated for the translative degrees of freedom. It was therefore decided to ignore the rotative degrees of freedom since the wrong radius of gyration might have been used. The agreement between *SMS* and the reference data is as seen very good, *Nemoh* is however showing some difference in amplitude for the RAO in heave. At one instance there is a case of "irregular frequencies", showing in Figure 19, which should be disregarded.

6.6 Response Amplitude Operators for a Series-60 Containership

The body plan and the main dimensions of the ship used in this section are presented in Figure 21 and Table 5. Result from the study of Kim (1999) is included, where the software *Wamit* acts as reference data in the validation process of *Nemoh*. The RAOs for heave and pitch are calculated in head seas at infinite depth. The reference data is published with the intention of validating a "unified" theory which is defined both as a strip theory contribution and a three-dimensional correction. The mathematical background to the "unified" method is described in Kim (1999).

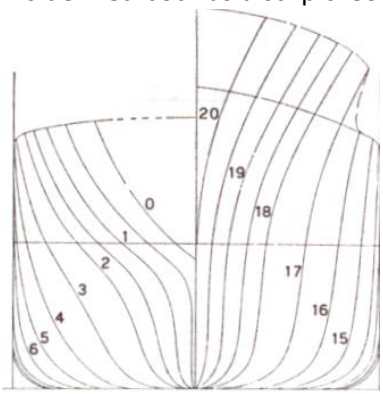

Figure 21: Body Plan of the Series-60 Containership

Table 4: Dimensions of the Series-60 Containership

LPP (m)	190.5
Breadth (m)	27.21
Draught (m)	10.89
Block-coefficient	0.7

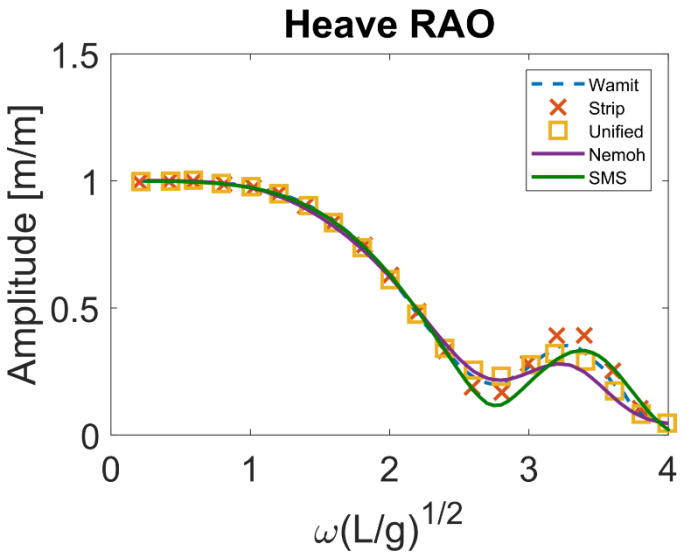

Figure 22: Heave RAO for Series 60 CB 0.7 ship with zero forward speed in head seas

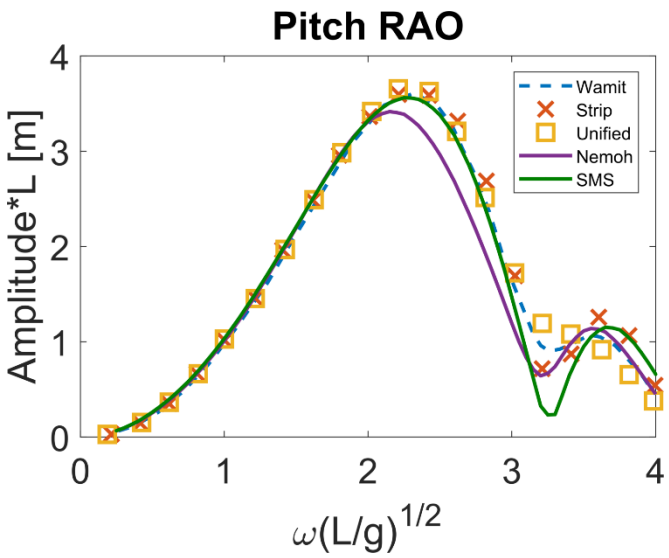

Figure 23: Pitch RAO for Series 60 CB 0.7 ship with zero forward speed in head seas

Result from the validation study is presented in Figure 22 & Figure 23. The ratio of $\frac{\lambda}{L} = 1$ is obtained at a nondimensional frequency of 2.42.

The obtained result from *Nemoh* shows favourable agreement with *Wamit*, however there exist a small shift in amplitudes for Pitch. *SMS* shows good agreement with *Wamit* in general, there is occurring a difference in amplitude for higher frequencies for both heave and pitch.

7. Further potential development of Nemoh

Potential areas of development and improvement of *Nemoh* is here addressed, some of which are identified with respect to the results presented from the validation study in Chapter 6. Relevant literature and mathematical theories are raised with the intention for users and developers to improve *Nemoh*.

7.1 Including Forward speed

Green´s function play a very important role when it comes to predicting wave induced responses, wave resistance and motions of a vessel advancing in waves. The three-dimensional Greens function method is easily computed for the problems without forward speed, in the case of forward speed, many theoretical and numerical difficulties appear such as double integrals and singularities (Hizir, et al. 2015). This chapter addresses relevant literature and methodology for ship motion predictions with forward speed.

There are mainly two different techniques that can be used to solve forward ship motion problems with Green´s function, namely (EFS) Exact Forward Speed and (AFS) Approximative Forward Speed (Hizir, et al. 2015). For the case of (EFS), the exact forward speed Green sources are used to satisfy forward speed boundary value problems. This is sometimes referred to as the Translating-Pulsating Source (TPS) method. The forward speed boundary conditions used in (TPS) are hard to satisfy and computationally demanding, although it has a more accurate formulation of the forward speed effects.

For the (AFS) technique, the boundary value problem is solved with Zero Forward Speed Green´s function but simplifications to capture the speed effects are applied. This method is often referred to as Pulsating Source (PS) method and will be discussed more in-depth since *Nemoh* utilizes Zero Speed Green´s function. The (PS) method discussed and addressed here is the one adopted by (Bailey, et al. 2001). The Pulsating Source method include forward speed through,

- Solutions computed at encounter wave frequency and not incident wave frequency
- Body-boundary conditions is solved with the assumption of having the steady- and unsteady motions de-coupled and having the steady motion represented by the free-stream velocity. Simplified “m-terms”, which represents the instantaneous submerged body, are included in the pitch-and yaw body boundary conditions
- The expression of Bernoulli´s equation can be written in terms of “m-terms”, a simpler variant of these may be included when calculating the added mass and damping coefficients.

To clarify, the (PS) Green’s function satisfies a zero-speed free-surface boundary condition but forward speed is included in a simplified manner in the linearized body-boundary condition and Bernoulli’s equation, i.e. the added mass and damping coefficients (Hudson 2018). While (TPS) Green’s function satisfies a linear free-surface boundary condition and therefore including better forward speed effects. In order for *Nemoh* to compute at encounter wave frequency and include “m-terms” in the

body-boundary condition, one would have to perform a major modification to the source code of *Nemoh*.

The following section explores the prospect of implementing the last-mentioned bullet point in an attempt to capture simplified speed effects in the hydrodynamic coefficients computed in *Nemoh*, referred to as an independent "speed-correction". This approach might be seen as a "*sensible approximation, and not quite the same as a pulsating source method in full*" - (Hudson 2018).

7.2 Speed corrected hydrodynamic coefficients

Commercial software's for seakeeping computations do often have the capability to compute with respect to a ship's forward speed. Since *Nemoh* was originally developed for computing wave loads on stationary offshore structures, it's not yet capable to run speed dependent simulations. This chapter explores the prospect of compensating for the velocity independency of *Nemoh* by adding a speed-correction to the added mass and damping coefficients, A_{ij} and B_{ij}. The corrections are fully presented in *Table 13, PNA III* Lewis (1989), and may be implemented as an independent post-processor to *Nemoh*. It is therefore assumed that the correction-principles used in Strip Theory also may be implemented in *Nemoh*. The speed dependency is included in other hydrodynamic coefficients but the added mass in yaw due to sway is here used as an example. In consequence, the first term in Equation (7.2.1) from Strip Theory may be represented by the first "zero-forward speed"- term in Equation (7.2.2).

$$A_{62} = \int x a_{22} dx - \frac{U_0}{\omega_e^2} B_{22}(\omega) \tag{7.2.1}$$

The second term is the so called "speed-correction" as presented in *Table 13, PNA III* (Lewis 1989). Further, $A_{62}^{U\neq 0}$ is the resulting speed dependent coefficient and $A_{62}^{U=0}(\omega)$ is the output from *Nemoh*.

$$A_{62}^{U\neq 0} = A_{62}^{U=0}(\omega) - \frac{U_0}{\omega_e^2} B_{22}^{U=0}(\omega) \tag{7.2.2}$$

In order to verify this assumption, a published seakeeping validation-study by Bailey et al. (2001) will serve as reference. Here the added mass and damping coefficients are predicted for the Series-60 hull form travelling at a Froude number of 0.20. Bailey et al. (2001) has not only included experimental data but also presented three different methods. "Method A" is a method to reduce the computational burden of single and double speed dependent integrals by modifying the Greens function. "Method B" centres on the development of a numerical scheme to evaluate a different more simpler formulation of Greens function. A "pulsating source method" has also been included, as mentioned in Chapter 7.1.

The comparison between the reference data and the implementation of "speed-correction", as stated in Equation (7.2.2), is presented in Figure 24. The implementation clearly shows that a "speed-correction" converges to the more reasonable result obtained from Method A, B and experimental studies. The original coefficients from *Nemoh* are computed with the incident wave frequency while the "speed-correction" contains the encountering frequency ω_e which is dependent on forward speed, direction and incident wave frequency as stated in Equation (2.1.13). The result from the study is fully presented in Appendix 2.

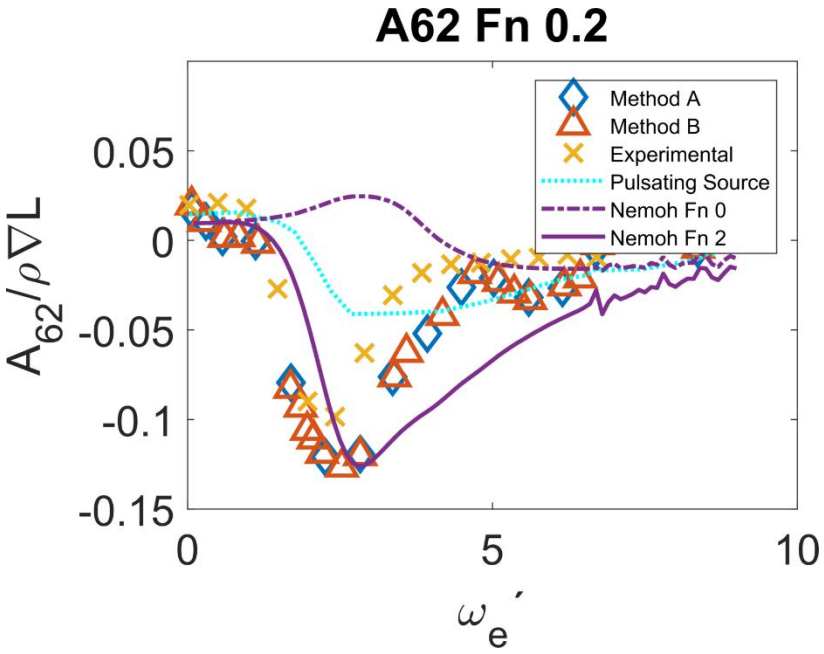

Figure 24: Added mass in yaw due to sway for Series-60 hull at Froude number 0.20

The nondimensional frequency vector ω_e' in Equation (7.2.3), is defined as the product between the encountering frequency and the square root of the fraction between the ships' length L, and the gravitational coefficient g.

$$\omega_e' = \omega_e \sqrt{\frac{L}{g}} \tag{7.2.3}$$

7.3 Irregular Frequencies

The occurring phenomena of irregular frequencies, addressed in Chapter 2.2 and identified in e.g. Figure 19, is here discussed with the intention of presenting relevant literature for handling the effects of irregular frequencies.

A straightforward approach with no alterations to the source code is given by Inglis and Price (1981), here the phenomena can be manually dealt with by interpolating the hydrodynamic coefficients in affected regions, a successful but time-consuming method.

A comprehensive approach with necessary alterations to source code is presented in the user's manual of *Wamit* (WAMIT 1999). Since the mathematical theory of *Wamit* is similar to *Nemoh,* it's solution for handling irregular frequencies is hereby shortly presented as a valuable approach. Further, the starting point is to discretize both the body surface and the interior free surface. The singularities arising from Green´s integral may be avoided by setting the panel size to the same order as the thickness, or smaller, in order to render the linear system well-conditioned.

Another approach, also presented in WAMIT (1999), is to represent the velocity potential by a distribution of dipoles only, without sources. The strength of the dipole will be equal to the difference of the two opposites side of the zero-thickness panel.

7.4 Parallel programming

The computational effort of *Nemoh* has been identified in Chapter 6.1 and further actions with the intention of lowering the computational time is hereby addressed. By using the *Matlab* wrapper one could implement the usage of the "parfor"-command, which executes for-loop iterations in parallel on workers in a parallel pool. Since the frequency dependent computations is in no way dependent on earlier results, loop iterations with different set of frequencies could be executed in parallel in a nondeterministic order. For computers with multiple cores, the only requirement for the implementation is to modify the *Matlab* wrapper of *Nemoh* so results from parallel-computations doesn't overwrite the same output-file.

The effect from a possible implementation, for a computer with two operating cores, could lower the computational time by 50%. For the case of a 6750-TEU with a resolution of 323 panels, as presented in Table 1, the computational time could be lowered to 25 from 50 seconds. This is still not comparable to a computational time of 1 second, as for the case of using *SMS*. The intention of addressing the computational effort of *Nemoh* is to raise the question and bring attention to the area for future releases.

8. Discussion

The presented material and results brings many interesting topics up for discussion, many of which the author himself eagerly demands explanation for. From the validation study presented in Chapter 6.4-6.5 it's been addressed that *Nemoh* differs quite significantly in amplitude in the case of Heave. While the RAO computed in heave from Chapter 6.6 corresponds really well to the reference data. One may distinguish that the calculated added mass in Figure 11 is overestimated for the same span of frequencies as the damping coefficients in Figure 13 is underestimated. If this is a generalized case, it might have significant impact on the results. In contrarily, a paper published by Parisella and Gourlay (2016) shows that the resulting RAO in Heave from *Nemoh* corresponds really well to the reference data computed in *Wamit* for three different ships.

In consequence to the diverse results, further studies are required in order to establish whether it's the case of inadequate input from the authors' side or lack of robustness in *Nemoh* that is the cause. This could be identified by other users of *Nemoh*, one approach is to participate in the benchmark study of Kim and Kim (2016), also presented in Chapter 6.4. By creating the hull-geometry from the presented body plan and computing hydrodynamic quantities with corresponding loading condition, the result may indicate what the cause for deviation is. By identifying whether it's a human error, lack of documentation in *Nemoh* or computational insufficiency is in anyway a contribution to further usage of *Nemoh*.

The scatter of results between methods for calculating RAOs where $\lambda \leq L$ (high frequencies), e.g. seen in Figure 15 and Figure 16, is of great interest to address. It seems that this area of frequencies is problematic for most types of simulation models. This could also be the explanation why seakeeping models are less accurate when the wavelength is less or close to the ships' length.

From the speed-corrected hydrodynamic coefficients published in Appendix 2, it's distinguishable that *Nemoh* overestimates the magnitudes for the added mass A_{26}, A_{35} and A_{53} from Figure 26, 28 and 30. In order to further determine the effects of this, one would have to compare excitation forces and RAOs from a Pulsating Source code which also utilizes a simplified approach to capture speed-effects.

9. Conclusions & Future work

An extensive study on the open source code *Nemoh* has been performed with the intention of contributing to further development. The mathematical theories behind BEM and Strip Theory are described and compared. The capabilities of *Nemoh* has been compared and validated to other sets of methods and results. This paper may act as a guideline to other users of *Nemoh* since the practical usage and structure have been properly identified. Chapter 7 might be useful for further development since concrete examples and areas of improvements are identified. The collection of literature can act as a basis for other studies within the area of hydrodynamics.

With respect to the results presented in Chapter 6, it's concluded that *Nemoh* requires much more computational time than a strip method while the accuracy of result is lower. No major improvements may therefore be achieved by substituting or implementing parts of *Nemoh* into *SMS*. *Nemoh* is however of use for the KTH Ship Dynamics Research Program and of other users of Lewis Method when establishing whether a hull-geometry is considered to be "too" unconventional for a two-parameter mapping technique or not. The capability to calculate the RAO in surge is also of interest for KTH Ship Dynamics Research Program since it's not a feature in *SMS*. Further, the approach to capture speed effects in the hydrodynamic coefficients is proven to be fairly accurate and could be of use for further development of *Nemoh.*

As discussed in Chapter 8 it's of interest for users to establish whether it's the case of inadequate input from the authors' side or lack of robustness in *Nemoh* that is the cause for the deviation in result. It's considered that *Nemoh* is not fully comparable with the accuracy and robustness of other software´s such as *Wamit* and *SMS*.

Future work has properly been identified in Chapter 7 where a potential speed dependency should be prioritized since it's of greatest interest for users worldwide.

10. Bibliography

Babarit, Aurélien, and Gérard Delhommeau. 2015. “Theoretical and numerical aspects of the open source BEM solver NEMOH.” Nantes, France: Proceedings of the 11th European Wave and Tidal Energy Conference (EWTEC2015).

Bailey, P.A, D.A Hudson, W.G Price, and P Temarel. 2001. *Comparisons between theory and experiment in a seakeeping validation study.* Transactions of the Royal Institution of Naval Architects 143.

Bandyk, Piotr Jósef. 2009. *A Body-Exact Strip Theory Approach to Ship Motion Computations.* Michigan: Naval Architecture and Marine Engineering in The University of Michigan.

Bertram, Volker . 2000. *Practical ship hydrodynamics.* Oxford: Butterworth-Heinemann.

de Jong. 1973. “Computation of the Hydrodynamic Coefficients of Oscillating Cylinders.” Delft: Netherlands Ship Research Centre TNO, Shipbuilding Department.

Faltinsen, O. M. 1990. *Sea Loads on Ships and Offshore Structures.* Vol. 1. Cambridge CB2 1RP, United Kingdom: Cambridge University Press.

Faltinsen, O.M, and F.C Michelsen. 1975. *Motions of Large Structures in Waves at Zero Froude Numbers.* Oslo: Det Norske Veritas.

Fossen, Thor I. 2011. *Handbook of Marine Craft Hydrodynamics and Motion Control.* UK: John Wiley & Sons, Ltd.

Hizir, Olgun, Zhi-Ming Yuan, Atilla Inceik, and Osman Turan. 2015. *The Effect of Forward Speen on Nonlinear Ship Motion Responses.* Glasgow, UK: Department of Naval Architecture, Ocean and Marine Engineering, Uniersity of Strathclyde.

Hudson, D.A, interview by Emil Andersson. 2018. “Pulsating Source code.” *E-mail conversation.* (16 May).

Inglis, R.B, and W.G Price. 1981. “Irregular Frequencies in Three Dimensional Source Distribution Techniques.” *International Shipbuilding Progress* 28 (319): 57-62.

Journée, J.M.J, and L.J.M Adegeest. 2003. *Theoretical Manual of Strip Theory Program "SEAWAY" for Windows.* Delft: Delft University of Technology, Ship Hydromechanics Laboratory.

Kim, Yonghwan. 1999. *Computation of Higher-Order Hydrodynamic Forces on Ships and Offshore Structures in Waves.* Massachusetts: Massachusetts Institute of Technology.

Kim, Yongwhan, and Jung-Hyun Kim. 2016. “Benchmark study on motions and loads of a 6750-TEU containership.” *Ocean Engineering* 119: 262-273. https://www.sciencedirect.com/science/article/pii/S0029801816300804.

Koskinen, Kristian. 2012. *Numerical simulation of shup motion due to waves and manoeuvring .* Stockholm: KTH, School of Engineering Sciences (SCI), Aeronautical and Vehicle Engineering, Naval Systems.

Lewis, Edward V. 1989. *Principles of Naval Architecture.* Vols. III, Motions in Waves and Controllability. Jersey City, NJ: The Society of Naval Architects and Marine Engineers.

McTaggart, Kevin. 2015. *Ship Radiation and Diffraction Forces at Moderate Forward Speed.* Canada: Defence Research and Development Canada.

McTaggart, Kevin. 2002. *Three Dimensional Ship Hydrodynamic Coefficients Using the Zero forward Speed Green Function.* Atlantic: Defence R&D Canada.

Newman, John Nicholas. 1977. *Marine Hydrodynamics.* Massachussets: The Massachussets Institute of Technology.

OceaNet. 2016. "Modelling methodologies for the assessment of the wake effect of a wave energy converter farm." Ireland. http://www.oceanet-itn.eu/wp-content/uploads/OceaNET-Final-Workshop-Nicolas-Tomey.pdf.

Ogilvie, T. Francis, and Ernst O. Tuck. 1969. *A Rational Strip THeory of Ship Motions: Part 1.* Michigan: Department of Naval Architecture and Marine Engineering, College of Engineering, The University of Michigan.

Ovegård, Erik. 2009. *Numerical simulation of parametric rolling in waves.* Stockholm: KTH Centre for Naval Architecture.

Palmquist, Mikael, and Jianbo Hua. 1995. *A Description of SMS - A Computer Code for Ship Motion Simulation.* Stockholm: Department of Vehicle Engineering Royal Institute of Technology, KTH.

Parisella, G, and T.P Gourlay. 2016. *Comparison of open-source code Nemoh with Wamit for cargo ship motions in shallow water.* Perth, Australia: Centre for Marine Science and Technology, Curtin University.

Rosén, Anders. 2011. *Ship motions in six degrees of freedom.* Stockholm: Centre for Naval Architecture KTH.

Salvesen, Nils, E. O. Tuck, and Odd Faltinsen. 1970. *Ship Motions and Sea Loads.* Oslo: Det Norske Veritas.

Soares, Carlos G. 2016. "Progress in Renewable Energies Offshore: Proceedings of the 2nd International Conference on Renewable Energies Offshore (RENEW2016)." Lisbon, Portugal.

Ursell, F. 1949. *On The Heaving Motion Of a Circular Cylinder On The Surface Of a Fluid.* Manchester: Department of Mathematics, The university.

WAMIT. 1999. *WAMIT User Manual Version 7.2.* User Manual, Massachussetts Institute of Technology.

Zachrisson, Daniel. 2011. *Manoeuvrability model for a Pure Car and Truck Carrier.* Stockholm: KTH, School of Engineering Sciences (SCI), Aeronautical and Vehicle Engineering, Naval Systems.

Appendix 1: Code Architecture & Geometry conversion

In order to simplify geometry conversions and pre-process hydrostatic quantities, a Matlab script from an introduction course to Marine Technology SD2725 at KTH, was implemented. The script was originally written by associate professor in naval architecture and manager of KTH Ship Dynamics Research Program, Anders Rosén. It has here been implemented with the purpose of finding vertical hydrostatic equilibrium for a ship and identifying relevant hydrostatic quantities. The ship-geometry is defined section-wise in a ".bri" format which was originally used in a naval architecture program called *Tribon.* The overall architecture of the code is summarized as a flowchart in Figure 25. The right-handed coordinate system *Oxyz* is initially defined with its origin in Centre of Gravity.

From the iterative process of finding hydrostatic equilibrium, it's feasible to obtain a ships' waterlines, i.e. the intersection between hull and water. This is further used in "Waterline hull-cut" where the submerged part of the geometry is stored.

In order to define quadrilateral panels, hull-offset points are distributed to sections with the objective of having a consistent number of points defined along the length of the ship. Sections where the points are scattered a great distance apart in the z-direction is identified by "Adding hull-offset points". Points are either added by linear interpolation or spline/linear interpolation. The results from a cubic spline interpolation is often uncertain due to the occasionally inconsistent structure of ".bri" files. Inconsistencies could for example be in the form of having a z-coordinate mapped to two different y-coordinates, resulting in even worse discontinuities with cubic interpolation. Linear interpolation is therefore utilized to keep the final error low.

"Quadrilateral panels" are now created by mapping four coordinates over two sections from bow to stern, creating four corners, oriented counter-clockwise, as seen from the fluid domain looking into the body. The information is stored in a four-dimensional matrix and act as input to "Mesh.m" for which defines the right input for *Nemoh*. The origin of z-axis is now defined at the water surface with the intention of simplifying calculation of the mass- and inertia matrix. In the current version of Nemoh, one should discard the inertia matrix that is provided by the "*Mesh.m*" tool and instead define it manually with respect to the actual axis of origin. By inspecting the generated mesh from "Mesh.m" one could distinguish faulty panels, the normal to the panel should be pointing into the surrounding fluid. While running *Nemoh* the frequency vector has to include values larger than zero.

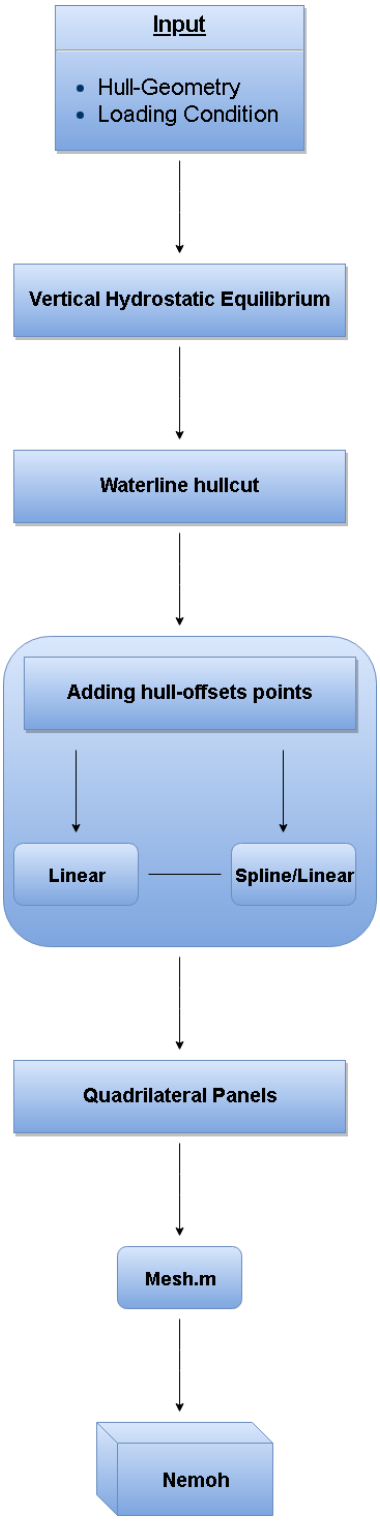

Figure 25: Flowchart of the code architecture

Appendix 2: Speed-corrected hydrodynamic coefficients

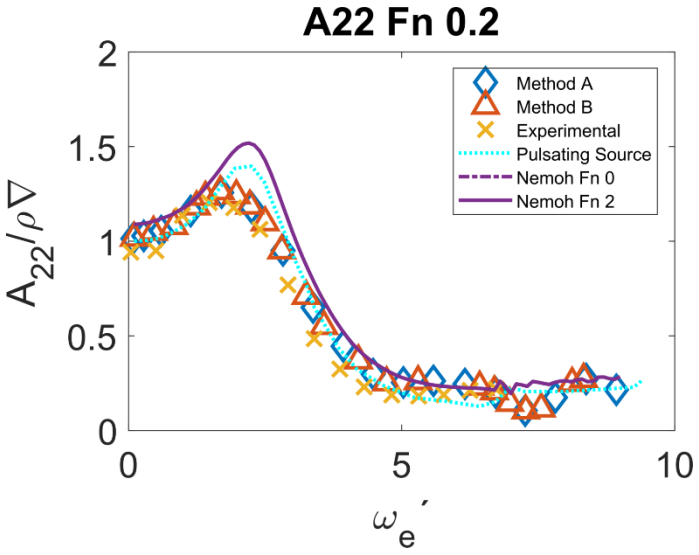

Figure 26: Added mass A_{22} for Series-60 hull at Froude number 0.20

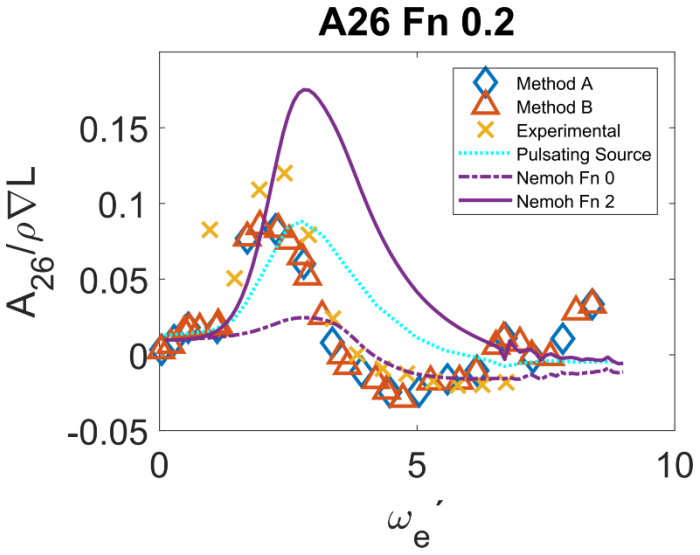

Figure 27: Added mass A_{26} for Series-60 hull at Froude number 0.20

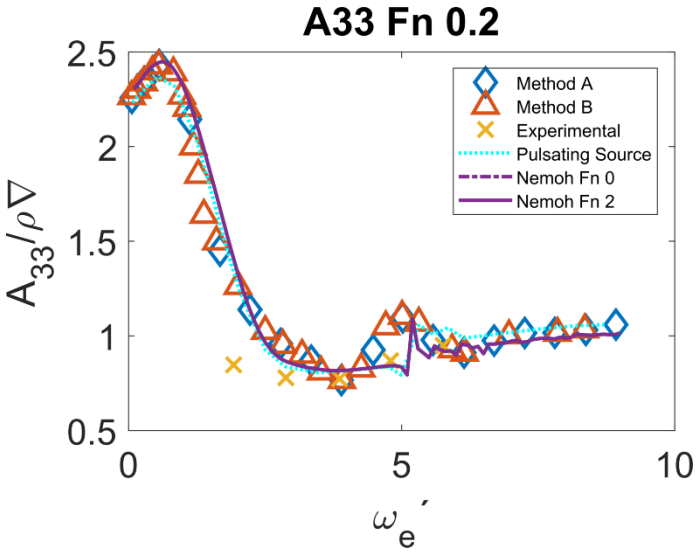

Figure 28: Added mass A_{33} for Series-60 hull at Froude number 0.20

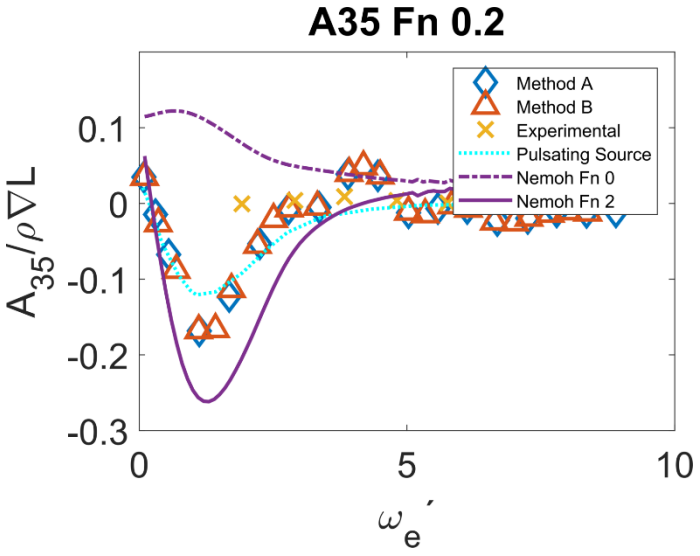

Figure 29: Added mass A_{35} for Series-60 hull at Froude number 0.20

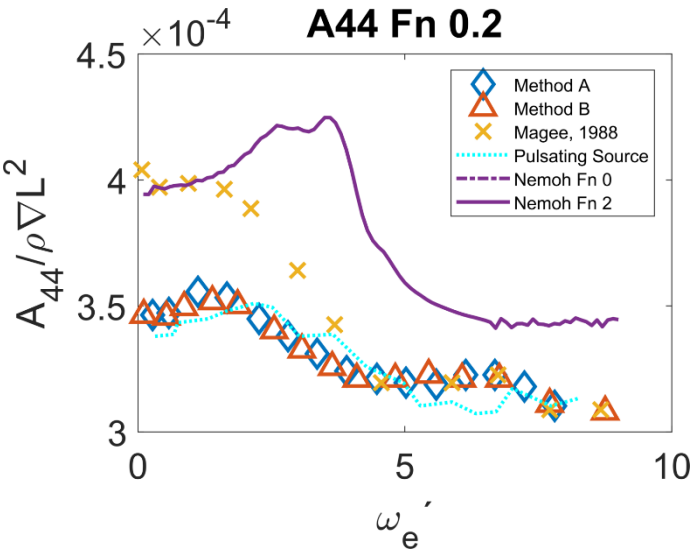

Figure 30: Added mass A_{44} for Series-60 hull at Froude number 0.20

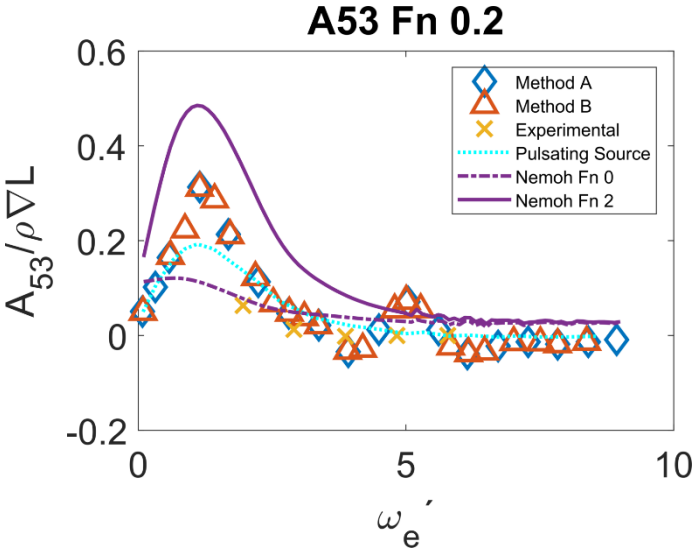

Figure 31: Added mass A_{53} for Series-60 hull at Froude number 0.20

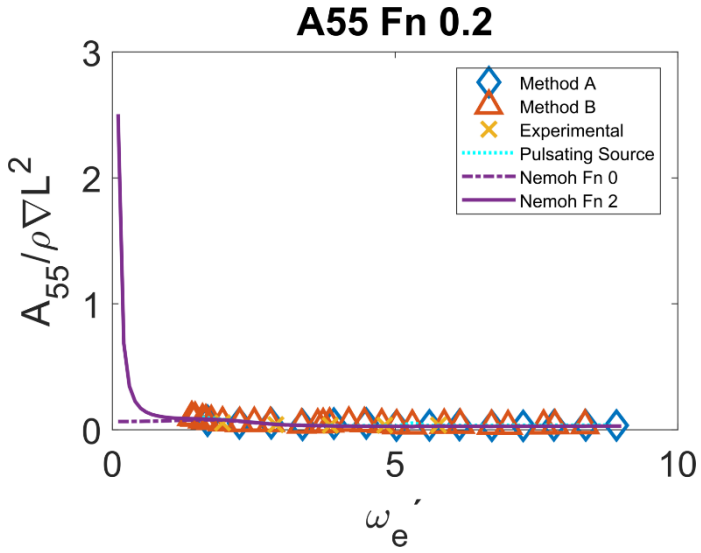

Figure 32: Added mass A_{55} for Series-60 hull at Froude number 0.20

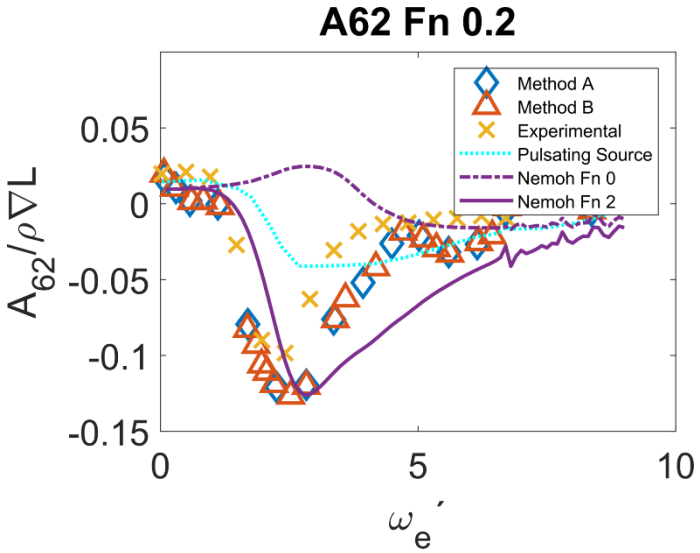

Figure 33: Added mass A_{62} for Series-60 hull at Froude number 0.20

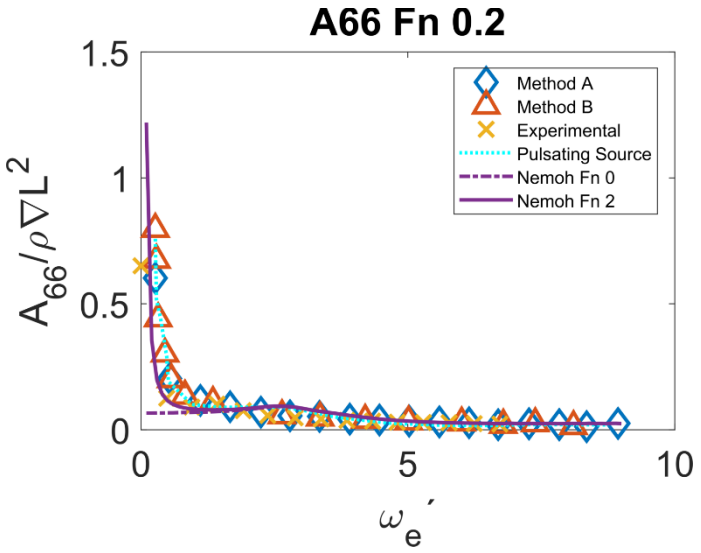

Figure 34: Added mass A_{66} for Series-60 hull at Froude number 0.20

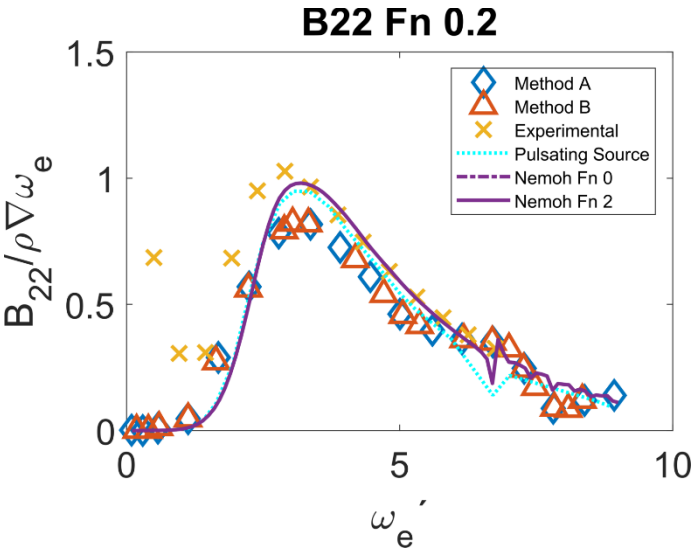

Figure 35: Added mass B_{22} for Series-60 hull at Froude number 0.20

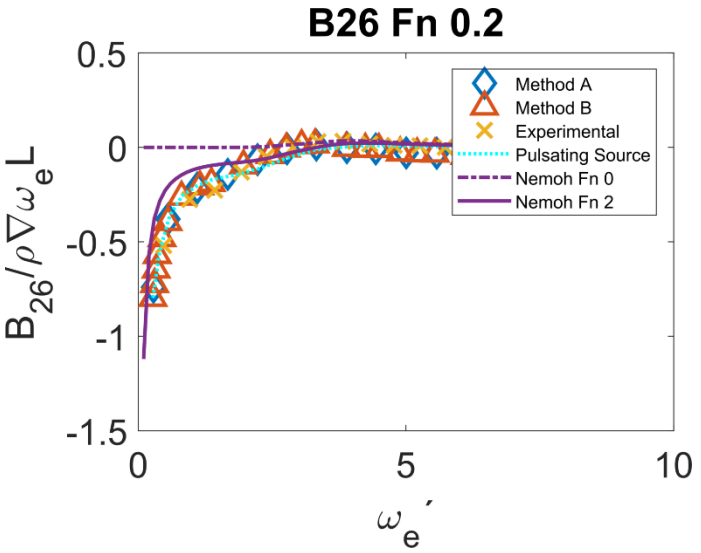

Figure 36: Added mass B_{26} for Series-60 hull at Froude number 0.20

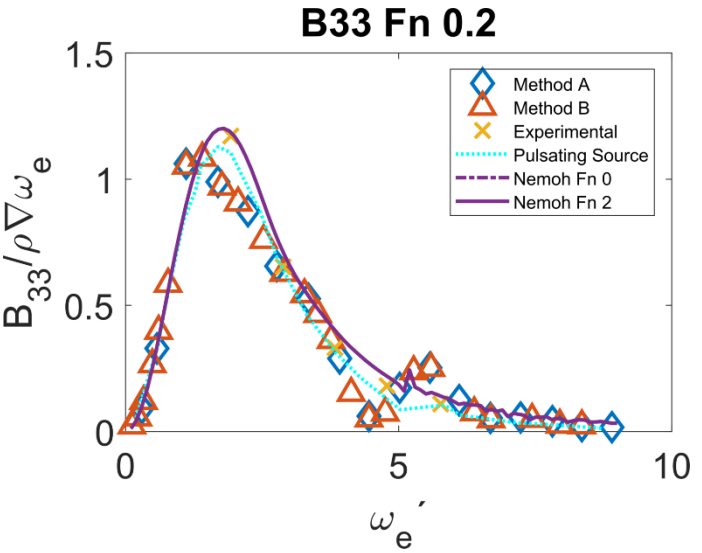

Figure 37: Added mass B_{33} for Series-60 hull at Froude number 0.20

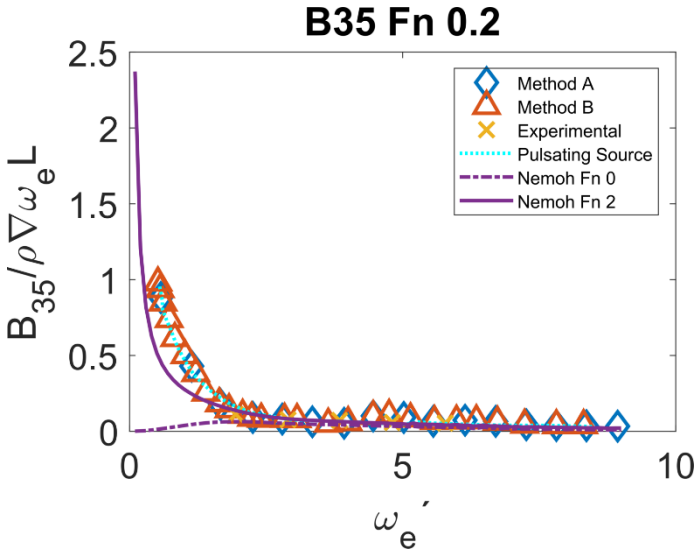

Figure 38: Added mass B_{35} for Series-60 hull at Froude number 0.20

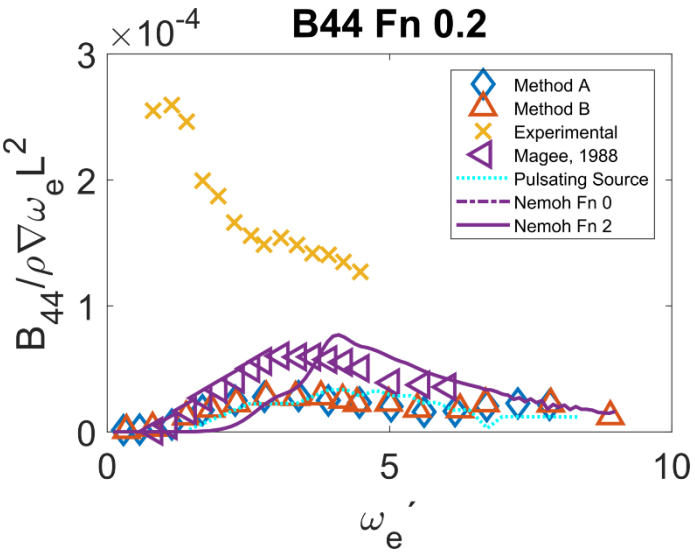

Figure 39: Added mass B_{44} for Series-60 hull at Froude number 0.20

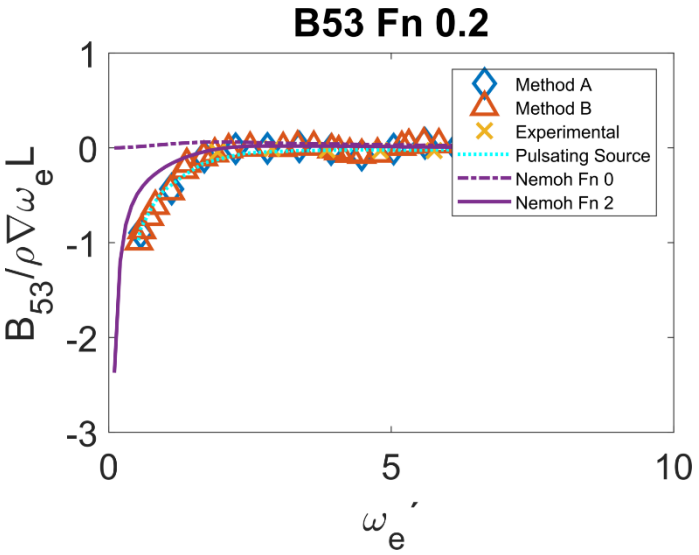

Figure 40: Added mass B_{53} for Series-60 hull at Froude number 0.20

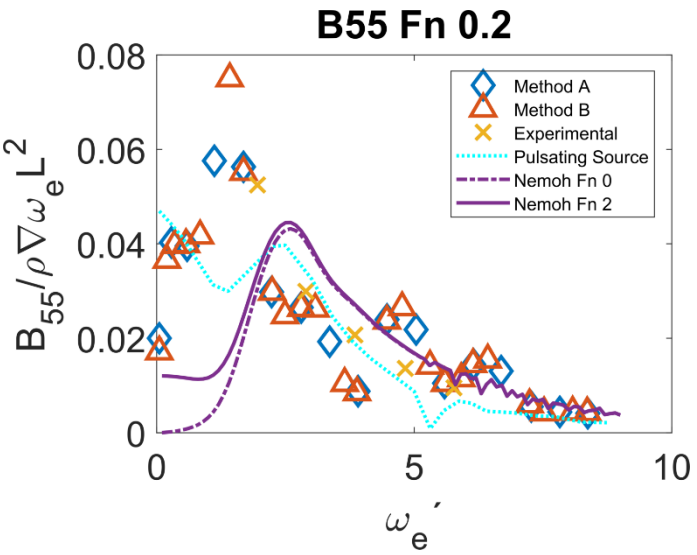

Figure 41: Added mass B_{55} for Series-60 hull at Froude number 0.20

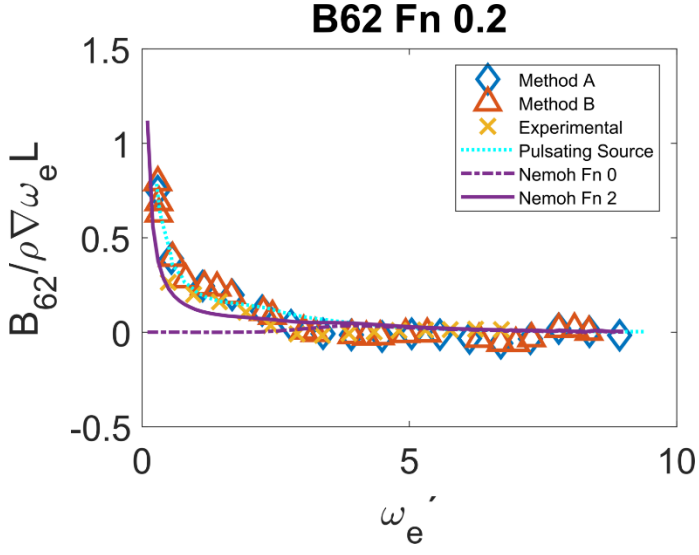

Figure 42: Added mass B_{62} for Series-60 hull at Froude number 0.20

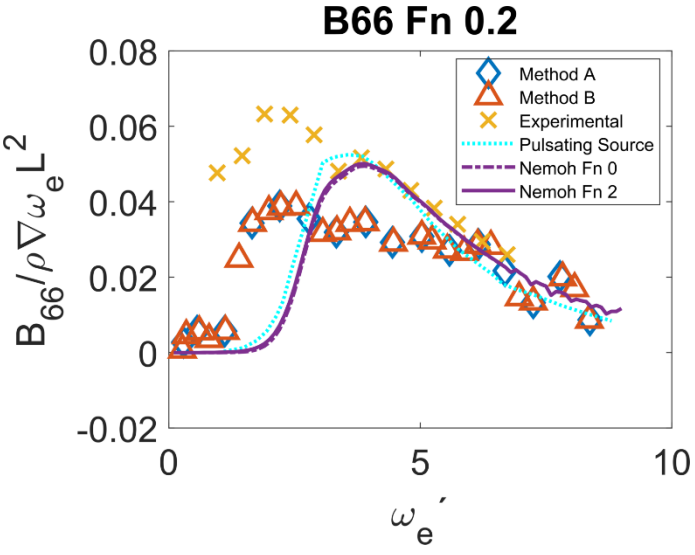

Figure 43: Added mass B_{66} for Series-60 hull at Froude number 0.20

TRITA TRITA-SCI-GRU 2018:274